Modifiers of genetic dominance at the Arabidopsis self-incompatibility locus retain proto-miRNA features and act through non-canonical gene silencing pathways

Rita A. Batista[1,a], Eléonore Durand[1], Monika Mörchen[1], Jacinthe Azevedo-Favory[2], Samson Simon[1], Manu Dubin[1], Vinod Kumar[3], Eléanore Lacoste[4], Corinne Cruaud[5], Christelle Blassiau[1], Matteo Barois[1], Anne-Catherine Holl[1], Chloé Ponitzki[1], Nathalie Faure[1], William Marande[6], Sonia Vautrin[6], Isabelle Fobis-Loisy[7], Jean-Marc Aury[4], Sylvain Legrand[1], Ute Krämer[3], Thierry Lagrange[2], Xavier Vekemans[1], Vincent Castric[1]

1. Univ. Lille, CNRS, UMR 8198 – Evo-Eco-Paleo, F-59000 Lille, France
2. CNRS, Laboratoire Génome et Développement des Plantes, UMR 5096, 66860 Perpignan, France, and Université Perpignan *Via Domitia*, Laboratoire Génome et Développement des Plantes, UMR 5096, F-66860 Perpignan, France
3. Department of Molecular Genetics and Physiology of Plants, Faculty of Biology and Biotechnology, Ruhr University Bochum, D-44801 Bochum, Germany
4. Génomique Métabolique, Genoscope, Institut François Jacob, CEA, CNRS, Univ Evry, Université Paris-Saclay, 91057 Evry, France
5. Genoscope, Institut François Jacob, CEA, Université Paris-Saclay, Evry, 91057, France
6. INRAE - CNRGV French Plant Genomic Resource Center - Castanet Tolosan, France
7. Laboratoire Reproduction et Développement des Plantes, Université de Lyon, ENS de Lyon, UCB Lyon 1, CNRS, INRAE, F-69342 Lyon, France

a. Current address: Max Planck Institute for Biology, Department of Algal Development and Evolution, 72076 Tübingen, Germany

Corresponding author: Vincent Castric, vincent.castric@univ-lille.fr

Author Contributions: Designed research – RAB, ED, MM, JA-F, MD, SS, VK, IF-L, MB, J-MA, SL, UK, TL, XV, VC; Performed research – RAB, ED, MM, JA-F, MD, SS, VK, EL, CC, CB, MB, A-CH, CP, NF, IF-L; Contributed new reagents or analytic tools – WM, SV, IF-L, J-MA, UK, TL, XV, VC; Analyzed data – RAB, ED, MM, JA-F, MD, SS, VK, EL, MB, J-MA, SL, XV, VC; Wrote the paper – RAB, VC. All authors reviewed and edited the manuscript.

Abstract

Self-incompatibility in flowering plants is a common mechanism that prevents self-fertilization and promotes outcrossing. In Brassicaceae, the self-incompatibility locus is highly diverse, with many alleles arranged in a complex dominance hierarchy and exhibiting monoallelic expression in heterozygote individuals. Monoallelic expression of the pollen self-incompatibility gene is achieved through the action of sRNA precursors that resemble miRNAs, although the underlying molecular mechanisms remain elusive. Here, we engineered *Arabidopsis thaliana* lines expressing components of the *Arabidopsis halleri* self-incompatibility system, and used a reverse genetics approach to pinpoint the pathways underlying the function of these sRNA precursors. We showed that they trigger a robust decrease in transcript abundance of the recessive self-incompatibility genes, but not through the canonical transcriptional or post-transcriptional gene silencing pathways. Furthermore, we observed that single sRNA precursors are typically processed into hundreds of sRNA molecules with a variety of sizes, abundance levels and ARGONAUTE loading preferences. Our results suggest that these seemingly arbitrary processing characteristics are essential for establishing the self-incompatibility dominance hierarchy, as they enable a single sRNA precursor from a dominant allele to effectively repress multiple recessive alleles, thus providing a unique example of how small RNAs mediate gene silencing within a highly complex regulatory network.

Graphical abstract

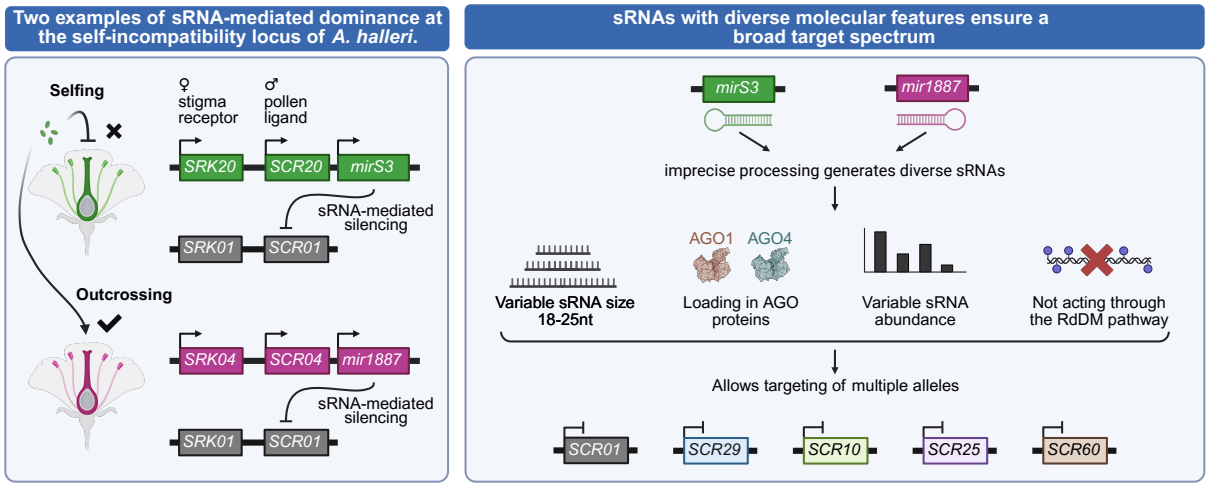

Main text

Introduction

Self-incompatibility is a widespread self-recognition mechanism in hermaphroditic flowering plants that prevents selfing and enforces outcrossing. In Brassicaceae, self-pollen recognition is controlled at the sporophytic level by a single non-recombining self-incompatibility locus (*S*-locus) containing two protein-coding genes: the female component encoding a trans-membrane receptor (SRK) expressed in papillae cells, and the male component consisting of an SCR peptide (referred to as SP11 in the Brassica nomenclature) produced in the anther tapetum and deposited on the surface of the pollen grains. The SRK and SCR proteins function as a receptor-ligand system, such that pollen germination is stopped when a pair of cognate SRK and SCR proteins interact upon pollen deposition on the pistil, ultimately preventing self-fertilization (1–5). The *S*-locus has been subject to an intense long-term balancing selection, which favors the maintenance of a high number of distinct *S*-alleles (6–9). Although heterozygosity is typically very high at the *S*-locus, monoallelic expression of the male *SCR* gene is the rule, following a transitive and mostly linear dominance hierarchy among *S*-alleles (10–12). These dominance interactions maximize reproductive success by ensuring that in a diploid individual only one of the two *SCR* alleles is expressed, thus preventing pollen rejection by females that share the same allelic specificity as the repressed, recessive *SCR*, and thereby increasing the number of compatible female partners (13). In *Arabidopsis lyrata* and *A. halleri*, respectively, 56 and 43 *S*-alleles have been documented so far (7, 14), which are divided into four main dominance classes - class IV being the most dominant and class I the most recessive (15, 16).

Underlying these dominance interactions are dominance modifiers - genetic elements dedicated to altering dominance relationships between other alleles in *trans* (17). In the particular context of the self-incompatibility system these dominance modifiers are located in the *S*-locus and take the form of sRNA-generating loci that are hypothesized to modulate the expression of the *SCR* gene_(18). Similarly to miRNAs genes, these loci are transcribed into an RNA molecule that is predicted to fold and form a hairpin structure, which is subsequently cleaved into sRNAs. In *A. halleri*, eight distinct families of sRNA precursors, defined based on sequence similarity, are predicted to regulate dominance interactions both between and within the four *S*-allele dominance classes (19). Interestingly, in Brassica where only two dominance classes exist, only two sRNA precursor families have been identified (12, 20, 21), suggesting that there is an association between the complexity of the dominance network and the total number of dominance modifiers. The two sRNA precursors of Brassica (*Smi* and *Smi2*) have each been suggested to produce a 24-nt sRNA with sequence similarity to the 5' region of *SCR.* The presence of this sRNA is associated with decreased expression of the recessive *SCR* allele, as well as deposition of DNA methylation within and around the targeted region in tapetum cells (12, 20, 21). This is reminiscent of what is observed in several plant species where 21/24-nt sRNAs derived from miRNAs genes or inverted repeats can be loaded onto proteins of the ARGONAUTE4 (AGO4) clade and subsequently elicit *de novo* DNA methylation at target loci, such as transposable elements or protein-coding genes, through the RNA-directed DNA Methylation

57 (RdDM) pathway (22–26). Similar mechanisms could be utilized by *Smi* and *Smi2*; nevertheless, this
58 hypothesis was never empirically tested.
59 In Brassica, the dominance hierarchy of *S*-alleles was proposed to rely on the combinatorial effect
60 of single nucleotide variants at the *Smi* and *Smi2* sequences and at their respective *SCR* target sites
61 (21). In Arabidopsis, where more dominance classes exist, the dominance network is hypothesized to
62 rely on two properties: i) recessive alleles carry more target sites and these sites are more generalist
63 (*i.e.* they are targeted by more sRNA precursors families than dominant alleles); and ii) sRNA
64 precursors of dominant alleles are more generalist (*i.e.* they target a higher number of alleles than those
65 sRNA derived from precursors in more recessive alleles) (19). Despite this observation, the molecular
66 features allowing sRNA precursors to target multiple alleles and have a broad targeting spectrum
67 remain to be identified. In addition, among the eight families of sRNA precursors previously predicted
68 to control the dominance hierarchy in Arabidopsis, only one has been subject to formal experimental
69 validation (19).
70 In this study, we aimed at identifying the molecular pathway underlying the sRNA-mediated
71 dominance interactions between *S*-alleles in Arabidopsis. To achieve this, we engineered and
72 characterized a series of *A. thaliana* lines recapitulating the self-incompatibility phenotype of *A. halleri*,
73 and used these lines to show that two different sRNA precursors from dominant *A. halleri S*-loci trigger
74 a decrease in abundance of recessive *SCR* transcripts. We thus provide direct proof that this
75 heterologous approach can be used to validate sRNA precursor function, both at the phenotypic and at
76 the molecular level. This system also allowed us to investigate if key components of the canonical
77 RdDM pathway, such as the ARGONAUTE proteins AGO4 and AGO6, and subunits of the DNA-
78 dependent RNA polymerases POLIV and POLV, are required for the repression of *SCR* transcript by
79 *S*-locus sRNA precursors, and our analyses demonstrate that the two selected sRNA precursors do not
80 act through the canonical RdDM pathway.
81 Additionally, we reveal that despite their structural similarity to miRNAs, *S*-locus-derived sRNA
82 precursors produce a large population of sRNAs with different sizes, sequences, ARGONAUTE loading
83 preferences and target sites. We show that this molecular heterogeneity is important to maximize the
84 number of targeted *S*-alleles, thus allowing one dominant allele to silence multiple recessive alleles at
85 the same time. Overall, our results show how the distinctive molecular features of *S*-locus sRNAs
86 contribute to effective gene silencing within a complex regulatory network, shedding light on their role
87 in shaping dominance interactions of an important reproductive phenotype.

88 **Results**

89 *The sRNA precursors Ah04mir1887 and Ah20mirS3 control dominance interactions at the S-locus by*
90 *decreasing the transcript level of the recessive SCR01 allele*

91 To study in detail the molecular mechanisms controlling the activity of dominance modifiers in the
92 self-incompatibility system of *A. halleri*, we first recreated the self-incompatibility reaction of *A. halleri* in
93 the selfing species *A. thaliana*, since the latter is a more tractable study model. To do this, we expressed
94 the *SRK01* receptor and its cognate *SCR01* ligand in female and male parents, respectively (19, 27,
95 28). Manual crosses between these plants revealed that the germination of pollen from a *SCR01*-

96 expressing male was abolished when deposited on pistils of an *SRK01*-expressing female, the hallmark
97 of a self-incompatible reaction **(Fig. 1C and D, WT panels)**. Given the challenges faced in prior studies
98 to reconstruct this reaction in the Col-0 ecotype, all *A. thaliana* plants used in this study are of the C24
99 ecotype, where the self-incompatibility can be faithfully recreated as shown both in this, and in other
100 studies (27, 29, 30).

101 Among the eight known families of *A. halleri* sRNA precursor loci, only one - mirS3 - has been
102 experimentally validated to regulate dominance between two distinct *S*-alleles: specifically, the
103 dominance of allele Ah20 over Ah01, mediated by Ah20mirS3 sRNAs, which target the *SCR01* intronic
104 region **(Fig. 1B)** (19). In this study, we set out to further investigate the molecular properties of
105 Ah20mirS3, as well as examine if the yet uncharacterized mir1887 family could also function as a
106 dominance modifier. For this, we focused on testing the role of the sRNA precursor Ah04mir1887 in
107 controlling the dominance of allele Ah04 over Ah01, whose sRNAs are predicted to target the promoter
108 region of *SCR01*, immediately upstream of the TSS **(Fig. 1A, Fig. 1 S1)**. We thus generated transgenic
109 lines expressing Ah04mir1887, introgressed this transgene into an *SCR01*-expressing male, and used
110 these plants to pollinate *SRK01*-expressing females, testing whether the presence of the Ah04mir1887
111 sRNA precursor locus could transform the previously incompatible interaction between *SCR01* and
112 *SRK01* into a compatible one **(Fig. 1C)**. In the particular case of Ah20mirS3, the transgenic line
113 previously generated by Durand et al. (19) and used here expresses both Ah20mirS3 and Ah20mir1887
114 because of their close physical proximity within the Ah20 allele **(Fig. 1B)**. To specifically isolate the
115 impact of Ah20mirS3 in the dominance interaction of Ah20 over Ah01, we developed the *SCR01*^{*mir1887}
116 transgenic line, which contains five point mutations designed to fully disrupt the slight homology
117 observed between some Ah20mir1887 sRNAs and *SCR01* **(Fig. 1B; Fig. 1 S2)**. We then used this
118 modified *SCR01*^{*mir1887} line for all subsequent tests on the functional role of Ah20mirS3.

119 We observed that combining either Ah04mir1887 (Interaction A), or Ah20mirS3 (Interaction B) with
120 *SCR01* results in a switch from an incompatible to a compatible pollen germination phenotype, which
121 is accompanied by a dramatic decrease in the abundance of the *SCR01* transcript, as measured by
122 RT-qPCR **(Fig. 1C and D, WT panels)**. This shows that both Ah04mir1887 and Ah20mirS3 act as
123 dominance modifiers in their respective allelic interactions, and that they accomplish this by decreasing
124 *SCR01* transcript abundance, thus preventing SRK-SCR cognate recognition and allowing pollen
125 germination to occur. Moreover, these results demonstrate that *SCR* transcript abundance can be
126 modulated by multiple sRNA precursor families that use distinct target sites in the *SCR* locus.

127 *Decrease in SCR01 transcript abundance does not depend on RdDM*

128 Next, we aimed at elucidating the exact molecular mechanism responsible for the reduction of
129 *SCR01* transcript abundance triggered by the two *S*-locus sRNA precursors. Given their resemblance
130 to miRNAs genes, one potential scenario is that sRNAs produced by Ah04mir1887 and Ah20mirS3
131 could trigger post-transcriptional gene silencing (PTGS) of the *SCR01* transcript. However, since these
132 sRNAs are predicted to target the promoter and intronic region of *SCR01*, and since the substrate of
133 PTGS is generally thought to be the mature mRNA (31), this does not support PTGS as the pathway
134 responsible for the decrease in *SCR01* transcript abundance. An alternative scenario is that

135 Ah04mir1887 and Ah20mirS3 sRNAs could trigger the RNA-directed DNA methylation pathway
136 (RdDM), resulting in the deposition of DNA methylation in their respective *SCR01* target sites, and
137 reduced *SCR01* transcription. Interestingly, previous studies have established that the silencing of
138 recessive alleles in the homologous self-incompatibility system of *Brassica* relies on sRNA-mediated
139 DNA methylation, although the specific pathway underlying this process remains elusive (12, 20, 21).
140 Thus, we focused our attention on the RdDM pathway, and set out to test if mutating key components
141 of this pathway would prevent Ah04mir1887 and Ah20mirS3 from reducing *SCR01* transcript
142 abundance. To circumvent the absence of RdDM mutant alleles in the C24 ecotype, we generated and
143 validated C24 *ago4 ago6* CRISPR/Cas9 mutant alleles **(Fig. 1 S3)**, and used the previously published
144 C24 *polIV* and *polV* knock-out alleles (32).
145 To our surprise, none of the RdDM mutants impaired the activity of the tested sRNA precursors. In
146 the case of Ah04mir1887 (Interaction A), *SCR01* transcript abundance was reduced in all mutant
147 backgrounds to a similar level as in wild type, which was reflected by a compatible pollen germination
148 phenotype **(Fig. 1C)**. Similarly, the presence of *Ah20mirS3* (Interaction B) was associated with a
149 decrease in *SCR01* transcript in all mutant backgrounds, showing that this sRNA precursor is still
150 functional when RdDM is impaired **(Fig. 1D)**. And while in the *ago4 ago6* mutant background the
151 reduction in *SCR01* transcript led to a compatible pollen phenotype, in both *polIV* and *polV* mutant
152 backgrounds the reduction in *SCR01* transcript level was sufficient to elicit a compatible pollen
153 phenotype **(Fig. 1D)**. This is likely explained by the fact that in Interaction B the basal *SCR01* transcript
154 level is increased in both *polIV* and *polV* mutant backgrounds when compared with wild type **(Fig. 1D,**
155 ***polIV* and *polV* panels vs. WT panel)**, pointing to an effect of these mutants on the expression of the
156 *SCR01* transgene. This suggests that the *SCR01*^{*mir1887} construct might be intrinsically targeted for
157 repression by RdDM, a phenomenon often observed in transgenic lines (33) (note that the *SCR01* and
158 *SCR01*^{*mir1887} transgenes used in Interaction A and B, respectively, correspond to two independent
159 transgenic lines with different insertion sites; **see Methods section**). Indeed, our data shows that a
160 strong reduction of *SCR01* transcript abundance is required for a compatible pollen germination
161 phenotype, since even very low levels of transcript can trigger an incompatibility reaction **(Fig. 1 S4)**.
162 Together, these results indicate that neither PTGS nor RdDM, at least not in their canonical forms,
163 appear to be responsible for the reduction in *SCR01* transcript abundance triggered by *S*-locus sRNA
164 precursors. Despite this, both Ah04mir1887 and Ah20mirS3 strongly and robustly decrease *SCR01*
165 transcript levels, which is necessary to abolish the self-incompatibility reaction, as shown here.

166 *Ah04mir1887 and Ah20mirS3 hairpins undergo heterogeneous processing to generate diverse sRNA*
167 *populations*

168 *S*-locus sRNA precursors, including those of the mir1887 and mirS3 families studied here, consist
169 of inverted repeats that are transcribed and predicted to form a RNA hairpin structure containing a 5'
170 arm, a terminal loop and a complementary 3' arm **(Fig. 2A)** (19), akin to the structures formed by
171 precursor miRNA (pri-miRNA) molecules. To delve deeper into the molecular properties of
172 Ah04mir1887 and Ah20mirS3, and to explore potential non-canonical pathways through which these
173 precursors may act, we conducted several sRNA sequencing experiments on both transgenic *A.*

174 *thaliana* and wild type *A. halleri* plants harboring Ah04mir1887 and Ah20mirS3. The resulting data
175 allowed us to compile a comprehensive database encompassing all sRNAs molecules sequenced for
176 each precursor, irrespective of their species origin. Using these data, we observed that dicing of *S*-
177 locus sRNA precursor hairpins leads to numerous sRNAs – at least 106 in the case of Ah04mir867, and
178 224 in the case of Ah20mirS3 **(Fig. 2B)**. These sRNAs range from 18 to 25 nt in length, with no clear
179 predominance of a specific length **(Fig. 2 S1 A-B)**, and their abundances vary by several orders of
180 magnitude **(Fig. 2B, Fig. 2 S1 C-D)**.

181 Given the large population of sRNAs produced by a single precursor, we aimed at evaluating the
182 functional relevance of each sRNA in controlling the abundance of the *SCR01* transcript. For this, we
183 used a previously published algorithm (19), which attributes a targeting score based on the homology
184 between a single sRNA and the *SCR* genomic region. A previous study has demonstrated that in
185 multiple *A. halleri S*-locus heterozygotes, a targeting score equal to, or above 18 is associated with
186 phenotypic dominance and a sharp decrease of the recessive *SCR* transcript level (10). Using this
187 algorithm, we found that 12 out of the total 106 sRNAs produced by Ah04mir1887, and 33 out of the
188 total 224 sRNAs produced by Ah20mirS3, have a base-pairing score of ≥ 18 and are thus predicted to
189 target *SCR01*. This subset of putatively functional sRNAs displays a variety of sizes and expression
190 levels **(Fig. 2B, see grey box)**.

191 To further assess whether these molecular features are reproducible between the native *A. halleri*
192 context and the transgenic *A. thaliana* context, we performed the same analyses as above, but using
193 only the sRNAs detected in *A. halleri* samples **(Fig. 2 S2)**. Although fewer sRNAs were identified in *A.*
194 *halleri*, their size distribution, abundances, and targeting spectrum closely mirror those observed in the
195 combined sRNA dataset from both species **(Fig. 2 S2 A-F)**. We hypothesize that the reduced number
196 of sRNAs detected in *A. halleri* is primarily due to the lower sequencing effort in this species compared
197 to *A. thaliana* **(Fig. 2 S2 G)***,* suggesting that the total number of sRNAs identified for each precursor is
198 highly dependent on sequencing depth, and that the saturation point was not reached in *A. halleri*.
199 Overall, these data indicate that the transgenic *A. thaliana* system accurately recapitulates the features
200 observed in the native *A. halleri* context, further supporting the use of *A. thaliana* as a more tractable
201 system to study the molecular bases of self-incompatibility reactions. Based on these findings, we
202 decided to proceed with the initially compiled sRNA database, which includes the sum of sRNAs
203 sequenced in both *A. halleri* and *A. thaliana*, for further downstream analyses in this manuscript.

204 To better understand the AGO loading preferences for each sRNA we performed AGO
205 immunoprecipitation (IP) assays, followed by sRNA sequencing in the Ah04mir1887 and Ah20mirS3 *A.*
206 *thaliana* transgenic lines. This showed that functional sRNAs (base-pairing score of ≥ 18) produced
207 from either precursor are loaded both into AGO1 (characteristic of the PTGS pathway) and AGO4
208 (characteristic of the RdDM pathway) **(Fig. 2 C-D)**. Notwithstanding this, a large part of these functional
209 sRNAs (75% in Ah04mir1887 and 48% in Ah20mirS3) are not found to be loaded in either of these two
210 AGO proteins, consistent with our observations that both the canonical PTGS and RdDM pathways are
211 unlikely to underlie the activity of these sRNA precursors. We also noted that the majority of sRNAs
212 loaded in AGO1 have a 5' terminal uracil, reflecting the known AGO1 preference for binding these

213 sRNAs (34). However, sRNAs loaded into AGO4, or with an unknown loading pattern, do not show a
214 significant bias towards a specific 5' nucleotide **(Fig. 2 S3)**.
215 Despite the structural similarity between *S*-locus sRNA precursors and miRNAs, and the existence
216 of shared features, such as the presence of mature 21-nt sRNAs and loading of some sRNAs into
217 AGO1, it is evident that *S*-locus sRNA precursors deviate from the typical characteristics associated
218 with canonical miRNAs, and cannot be characterized as such. Instead, our data show that Ah04mir1887
219 and Ah20mirS3 have an unusually staggered hairpin processing pattern with numerous sRNAs derived
220 from both the 5' and 3' arms, which differ in size, abundance level and ability to associate with AGO
221 proteins.

222 *Heterogeneous processing of S-locus sRNA precursors allows targeting of multiple S-alleles*

223 We hypothesized that this heterogeneity in hairpin processing pattern could play an important role
224 in the context of the complex *S*-locus dominance hierarchy by allowing a single sRNA precursor to exert
225 dominance over multiple other alleles. To test this, we expanded our analysis of the function of
226 Ah04mir1887 and Ah20mirS3 beyond the interaction with allele Ah01, and looked at their role within
227 the *A. halleri* dominance network **(Fig. 3)**.
228 We compiled previously published phenotypic data obtained by controlled reciprocal crosses
229 between different *A. halleri S*-locus heterozygotes to determine the position of allele Ah20 and Ah04 in
230 the dominance hierarchy of a total of 15 *S*-alleles **(Fig. 3)** (10, 19, 35). From this, we inferred that Ah20
231 is dominant over 13 other *S*-alleles, with 10 of these interactions relying on the action of Ah20mirS3
232 **(Fig. 3)**, as determined by the sRNA-*SCR* targeting algorithm described above. Thus, Ah20mirS3 is not
233 only able to mediate the repression of *SCR01*, but also the repression of at least nine other distinct
234 *SCR* alleles. Similarly, Ah04mir1887 mediates the repression of at least five different *SCR* alleles that
235 are recessive to Ah04 **(Fig. 3)**.
236 To test if the large population of sRNAs produced by these *S*-locus precursors is important in
237 repressing multiple target alleles, we examined the role of each individual sRNA produced by both
238 Ah04mir1887 and Ah20mirS3 **(Fig. 4)**: 11% of Ah04mir1887 sRNAs **(Fig. 4A, cluster 1)**, and 26% of
239 Ah20mirS3 sRNAs **(Fig. 4B, cluster 1)** are predicted to target at least one *SCR* allele within the inferred
240 dominance network presented in **Figure 3**. As is the case in Interaction A and B, there does not seem
241 to be a clear correlation between abundance and sRNA functionality in any of the analyzed interactions
242 **(Fig. 2B and Fig. 4, see cluster 1 vs. cluster 2)**. Nevertheless, sRNAs that are predicted to be
243 functional have a larger size (median of 23 nt vs. 21 nt), and in the case of Ah20mirS3, this is also
244 associated with a larger number of sRNAs being loaded in AGO proteins **(Fig. 4, see cluster 1 vs.**
245 **cluster 2).** Additionally, according to our sRNA-*SCR* targeting algorithm, most *S*-alleles are redundantly
246 targeted by multiple sRNAs **(Fig. 4)**.
247 When investigating in more detail the positional correspondence between sRNAs and the
248 Ah04mir1887/Ah20mirS3 precursor hairpin structure we noticed that sRNAs are produced in similar
249 amounts from both the 5' and the 3' arms of the hairpin **(Fig. 5)**. Each hairpin arm produces numerous
250 sRNAs that show a staggered pattern, suggesting imprecise dicing and resulting in a population of
251 sRNAs that show only a few nucleotide differences between them. In the case of Ah04mir1887, only

252 the sRNAs produced from the 5' hairpin arm are predicted to be functional against the *S*-alleles tested
253 here **(Fig. 5A)**. Remarkably, in the case of Ah20mirS3, each hairpin arm shows functional specialization
254 since sRNAs from the 5' arm target all allele classes except Class IV, while sRNAs from the 3' arm
255 exclusively target Class IV and Class III alleles **(Fig. 5B)**. Together, these observations suggest that
256 the high number and heterogeneous processing of sRNAs is a conserved and important feature of *S*-
257 locus sRNA precursors which allows targeting of multiple alleles and thus underlies their generalism.

258 **Discussion**

259 *S-locus sRNA precursors act through non-canonical gene silencing pathways*

260 Our characterization of self-incompatibility transgenic lines of *A. thaliana* contributes additional
261 evidence to the work of Durand et al. (19): collectively, these studies not only establish *A. thaliana* as a
262 tractable system to study dominance interactions among *A. halleri S*-alleles, but also experimentally
263 validate the role of two distinct sRNA precursor families in these interactions, even if the precise
264 mechanisms underlying their action remain elusive. Our study reveals that some of the sRNAs
265 generated in the processing of the *S*-locus sRNA precursors have a length of 24 nt and are loaded into
266 AGO4, potentially indicating a role for RdDM. Nevertheless, *ago4 ago6*, *polIV* and *polV* mutations did
267 not significantly affect the action of *A. halleri S*-locus sRNA precursors, suggesting that canonical RdDM
268 is not the primary mechanism through which Ah20mirS3 and Ah04mir1887 mediate the reduction in
269 *SCR01* transcript levels. While these results strongly suggest against DNA methylation as the basis of
270 this transcriptional modulation, it would be interesting to directly measure DNA methylation at the
271 *SCR01* locus using bisulfite sequencing or similar methods. However, such analyses remain
272 challenging because dominance is established during early pollen development, specifically in tapetum
273 cells, which are embedded within the anthers and difficult to isolate.
274 Considering their hairpin structure and their ability to also generate AGO1-loaded 21-nt sRNAs, it
275 could also be envisioned that these precursors could act through PTGS. Still, the location of target sites
276 in the promoter and intronic regions of *SCR01* poses a conundrum, since PTGS is reported to occur in
277 the cytoplasm, using mature mRNA as a cleavage substrate (31). Notably, in animals, several lines of
278 evidence point to miRNAs acting both in the cytoplasm and in the nucleus, with effects at the
279 transcriptional and post-transcriptional levels (36–38). In plants, it has been observed that an inverted
280 repeat targeting the intron of the soybean gene *FAD12-1A* triggers cleavage of its precursor mRNA
281 (pre-mRNA) in the nucleus, which is accompanied by accumulation of siRNAs of the cleaved pre-mRNA
282 (39). Additionally, all main miRNA processing components, including AGO1, are present in the nucleus
283 (40–42). Thus, given the independent slicer activity of AGO1 (43), it could be hypothesized that this
284 ARGONAUTE uses sRNAs to target the *SCR01* pre-mRNA in the nucleus, promoting its cleavage co-
285 transcriptionally. Alternatively, the interaction between AGO1 and the *SCR* pre-mRNA could promote
286 disassembly of the PolII complex leading to the arrest of transcription, as has been suggested to occur
287 in some miRNA genes upon salt stress (44). Even though we could not detect any siRNAs
288 corresponding to the cleavage of the *SCR01* pre-mRNA in any of our sRNA sequencing experiments
289 (data not shown), future experiments should investigate the possibility that the sRNA precursors at the
290 *S*-locus could act through nuclear PTGS or through transcriptional arrest.

291 Our results indicating that Ah20mirS3 and Ah04mir1887 work through an RdDM-independent
292 pathway contrast with previous observations in Brassica: in this latter system, the sRNA precursors *Smi*
293 and *Smi2* are associated with deposition of DNA methylation in and around the *SCR* target site and a
294 decrease in *SCR* expression (12, 20, 21). This could be a result from a direct incorporation of *Smi* and
295 *Smi2* sRNAs into AGO4-clade proteins which would elicit *de novo* DNA methylation through the RdDM
296 pathway, as has been observed for selected miRNAs and inverted repeats (22–26). Alternatively, as
297 suggested by Finnegan et al. (45), it could depend on *Smi*-induced cleavage of an antisense transcript
298 at the *SCR* locus, generating sRNAs that could subsequently be co-opted into the RdDM pathway.
299 Even though empirical investigations are still necessary to test these hypotheses in Brassica, the
300 cumulative evidence from these earlier studies and our stud suggests that different sRNA precursors
301 within the Brassicaceae self-incompatibility system can recruit distinct effector pathways, that
302 nevertheless converge into the same molecular phenotype: reduction of *SCR* transcript abundance.
303 This would imply that these regulatory elements have an outstanding molecular flexibility, despite
304 functioning within the specific evolutionary constraints of the self-incompatibility system. Thus, it cannot
305 be excluded that different *A. halleri* sRNA precursors, as well as precursors from other self-incompatible
306 species such as *A. lyrata* and *Capsella grandiflora* could use different gene regulatory pathways. Future
307 investigations of different *S*-locus sRNA precursor families in these species, using heterologous
308 expression systems as done in this study, or in the native context whenever genetic transformation is
309 feasible, will hopefully help answer this outstanding question.

310 *The complex S-allele dominance network relies on the unique features of S-locus sRNA precursors*

311 Durand et al. (19) previously showed that the *S*-locus sRNA precursors of *A. halleri* have high
312 generalism, and suggested that dominant *S*-alleles in particular, rely on this feature to target multiple
313 recessive alleles, rather than on carrying an increased number of sRNA precursors. Our study uncovers
314 the molecular basis for this generalism, and shows that the apparent haphazardous processing of *S*-
315 locus sRNA precursors is required to generate numerous functional sRNAs that target multiple alleles
316 cooperatively: remarkably, all *SCR* alleles analyzed in this study are targeted by multiple sRNAs of a
317 single sRNA precursor, and/or are targeted by distinct sRNA precursors. This contrasts with the less
318 complex dominance hierarchy of Brassica, where fewer allelic interactions are present, and a single
319 functional sRNA molecule per precursor has been suggested to mediate all dominance relationships
320 (20, 21). It is important to note that while we investigated a total of 15 *S*-alleles in this study, at least 43
321 are known to exist in *A. halleri* (7), and > 80 in the closely related *Capsella grandiflora* (14). Therefore,
322 in this study we most likely underestimated the fraction of functional sRNAs in each precursor, since
323 those that are non-functional in the allelic interactions explored here could potentially have a role in
324 interactions that have not yet been characterized.
325 Overall, the evidence suggests that collaborative targeting, either by multiple sRNAs of a single
326 precursor, or by sRNAs from distinct sRNA precursors, is an essential feature of this system: firstly, it
327 is essential for granting an *S*-allele its complete targeting spectrum against the many *S*-alleles
328 segregating in the population; and secondly, the use of multiple sRNAs with distinct molecular features
329 could trigger diverse effector pathways acting on the same target allele, which could perhaps underlie

330 the robust reduction of recessive *SCR* transcripts observed in all allelic interactions studied thus far
331 (this study and (10)).
332 Intriguingly, this resembles the collaborative non-self recognition model seen in Solanaceae, where
333 each self-incompatibility allele contains multiple *SLF* genes. SLF proteins are essential for recognizing
334 and neutralizing non-self S-RNases - female-derived ribonucleases that would otherwise inhibit pollen
335 germination. In this system, the presence of multiple *SLF* genes within a single *S*-locus allele - each
336 capable of recognizing a distinct S-RNase allele - together with the ability of some SLF proteins to
337 recognize and detoxify multiple S-RNases (generalism), is crucial. Both these features ensure a broad
338 recognition spectrum for each *S*-allele, preserving the complex network of inter-allelic interactions within
339 Solanaceae (46). While SLF generalism in Solanaceae likely relies on the ability of each of these
340 proteins to interact with multiple distinct S-RNases (47), sRNA precursor generalism in *A. halleri* relies
341 on their unique molecular features, specifically their ability to produce numerous sRNAs with distinct
342 targeting spectra.

343 *S-locus sRNA precursors provide a window into the miRNA evolution continuum*

344 Although sharing some structural similarities with miRNAs, the features of *S*-locus sRNA precursors
345 more closely resemble those of proto-miRNAs (48). Proto-miRNA loci are inverted repeats present in
346 several plant genomes that have acquired transcriptional competence, forming long hairpins which can
347 be diced by multiple Dicer-like proteins (DCLs), leading to a complex and heterogeneous population of
348 sRNAs (48–52). There is little evidence that such a sRNA population could cause substantial effects in
349 gene expression, at least through the canonical PTGS pathway; therefore, these structures have been
350 mostly regarded as substrates for selection to act on, rather than having immediate biological
351 significance (48–52). We hypothesize that the specific selective constraints of the *S*-locus dominance
352 network have likely contributed to the persistence of proto-miRNA features over extended evolutionary
353 times, and prevented their progression towards canonical miRNA features, as this would likely render
354 them unable to effectively target multiple *S*-alleles. It would be interesting to test if apparently stabilized
355 proto-miRNAs are also used in other biological systems where the expression of multiple genes/alleles
356 needs to be coordinated by a single regulator and under similar evolutionary constraints as those acting
357 on the *S*-locus. The mimicry of wing patterns in *Heliconius* butterflies would be an interesting model
358 system to test this, since balancing selection has favored the appearance of numerous alleles of the
359 supergene controlling wing pattern, and dominance relationships between them are prevalent (53, 54).

360 **Materials and Methods**

361 *Plant material & growing conditions*

362 Wild type (wt) and transgenic *Arabidopsis thaliana* plants used in this study were grown in a
363 greenhouse, using standard growth conditions (16 h light/8 h dark; 110 µmol/s/m2; 21°C; 70%
364 humidity). Seeds were germinated directly on soil, or in MS-medium (0.43% MS-salts, 0.8% Bacto agar,
365 0.19% MES hydrate, and 1% sucrose) when antibiotic selection was necessary for transgene selection.
366 Because the self-incompatibility reaction cannot be faithfully reconstructed in the *A. thaliana* Col-0
367 ecotype (27–30) all wild type and mutant plants used in this study were of the C24 ecotype. *polIV* and

368 *polV* correspond to the previously published and validated *rdm5 (nrpd1a)* and *rdm6 (nrpd1b*) mutant
369 alleles (32). These two mutants were generated in the *ros1* mutant background, which was removed in
370 our study by backcrossing to wt C24 plants. The *ago4 ago6* double mutant was generated in the C24
371 background using CRISPR/Cas9 **(see section *Generation and validation of CRISPR/Cas9 mutants*
372 for more details)**.
373 To obtain the *S*-allele sequences of Ah65, Ah60, Ah03, Ah33 and Ah19, five *Arabidopsis halleri*
374 individuals containing a combination of these alleles were collected from diverse natural European
375 populations (55), and grown under standard greenhouse conditions in order to obtain plant material for
376 DNA extraction and sequencing **(see the section *DNA extraction, Nanopore sequencing and*
377 *assembly of S-alleles* for more details)**. Following Goubet et al. (15), we further obtained the S-allele
378 sequence of Ah01, Ah02 and Ah25 by constructing and screening BAC libraries from fresh leaf samples,
379 and fully sequencing the positive clones using PACBIO.

380 *Cloning*

381 Several transgenic lines were used in this study: lines carrying SRK01, SCR01, and the sRNA
382 precursor Ah20mirS3 were cloned as detailed previously (19).
383 The precursors Ah20mir1887 and Ah20mirS3 are in very close physical proximity within the Ah20
384 allele, and the previously published Ah20mirS3 line contains both sRNA precursors (19). While
385 performing sRNA sequencing of AGO-IP experiments **(see section *ARGONAUTE*
386 *immunoprecipitation and sRNA sequencing*)**, we noticed that some Ah20mir1887 sRNAs show
387 homology to the 5' region of *SCR01*. The base-pairing score of these predicted interactions varies
388 between 12.5 and 18.5, depending on the sRNA **(see the section *sRNA database construction and*
389 *target site inference for Ah04mir1887 and Ah20mirS3* for more details on these scores)**. To
390 confidently isolate the effect of Ah20mirS3 in the dominance interaction of Ah20 over Ah01 (Interaction
391 B), we introduced five point mutations in the SCR01^{*mir1887} sequence that disrupt the homology with the
392 Ah20mir1887 sRNAs, rendering the Ah20mir1887 target site non-functional. The SCR01^{*mir1887}
393 transgene was generated by performing site-directed mutagenesis on the already published SCR01
394 clone (19), using the primers detailed in **table S1**. The resulting amplicon was then recombined into the
395 entry vector pDONR-Zeo, and subsequently recombined into the pB7m34GW destination vector using
396 the 3-fragment Gateway Cloning System (Invitrogen), including 5' and 3' mock sequences, as detailed
397 previously (19).
398 Ah04mir1887 was cloned by amplifying a region spanning this sRNAs precursor and containing 2
399 kb of upstream and downstream sequences from a BAC clone carrying allele Ah04, using the primers
400 detailed in **table S1**. The resulting amplicon was then recombined into the entry vector pDONR-Zeo,
401 and subsequently recombined into the pH7m34GW destination vector using the 3-fragment Gateway
402 Cloning System (Invitrogen), including 5' and 3' mock sequences, as detailed previously (19).
403 Arabidopsis thaliana C24 plants were transformed using the floral dip method (56), and transgenic
404 lines were selected using the appropriate antibiotics.

405 *Generation and validation of CRISPR/Cas9 mutants*

406 Given the aforementioned limitation that the self-incompatibility reaction of *A. halleri* can only be
407 reconstituted in the *A. thaliana* C24 ecotype (27–30), we created the *ago4 ago6* RdDM mutants in this
408 specific ecotype using CRISPR/Cas9. The expression cassette of pCBC-DT1T2 (57) was amplified
409 using two overlapping forward and reverse primers that contained two gene-specific sgRNA sequences
410 (Fw1: 5'-ATATATGGTCTCGATTGNNNNNNNNNNNNNNNNNNNGTT-3'; Fw2: 5'-
411 TGNNNNNNNNNNNNNNNNNNNGTTTTAGAGCTAGAAATAGC-3'; Rv1: 5'-
412 ATTATTGGTCTCGAAACNNNNNNNNNNNNNNNNNNNNCAA-3'; Rv2: 5'-
413 AACNNNNNNNNNNNNNNNNNNNCAATCTCTTAGTCGACTCTAC-3', where N corresponds to the
414 gene-specific gRNAs **(table S1)**, and underlined regions correspond to BsaI restriction sites). The
415 amplicons obtained from this PCR reaction were gel-isolated and inserted into pHEE401E (58) using
416 BsaI and T4 ligase (Thermo Fisher Scientific). The pHEE401E vectors containing gRNAs against *AGO4*
417 and *AGO6* were transformed into the *Agrobacterium tumefaciens* strain GV3101. The floral-dip method
418 (56) was then used to transform wt C24 *A. thaliana* plants.

419 To screen for T1 mutant plants, the regions targeted by the gRNAs were Sanger sequenced to
420 identify *ago4 ago6* mutants with premature stop codons in both genes **(Fig. 1 S3)**. In the T2 generation,
421 double homozygous mutants that did not carry the pHEE401E were selected by genotyping **(see table**
422 **S1 for primers)**.

423 To confirm that *ago4 ago6* mutations impair DNA methylation, a Chop-PCR assay was performed
424 (59). Briefly, this assay uses genomic DNA treated with the methylation-sensitive enzyme HaeIII as a
425 template for PCR. Primers targeting regions known to have AGO4/AGO6-dependent DNA methylation,
426 as well as control unmethylated regions are amplified **(see table S1 for primers)**. Using this method,
427 we could determine that the *ago4 ago6* mutant generated in this study shows reduced DNA methylation
428 levels, as has been previously published for other mutant alleles of these genes **(Fig. 1 S3 C)** (60).

429 *Pollen germination assays*

430 All lines used for the reconstruction of the self-incompatibility reaction in *A. thaliana* were used in
431 hemizygous state to mimic the abundance of sRNA precursors, and *SCR/SRK* in *A. halleri* individuals
432 heterozygous at the *S*-locus. Genotyping of each transgenic line/mutant was done by classical PCR, or
433 using the KASPar assay (61) **(table S1)**. Paternal plants hemizygous for *SCR01* and sRNA precursors
434 were obtained by crossing *SCR01* to Ah04mir1887 homozygous lines or by crossing *SCR01*^{*mir1887} to
435 Ah20mirS3 homozygous lines.

436 To assess the self-incompatibility reaction at the phenotypic level, pollen germination assays were
437 performed on manually crossed plants. Maternal plants hemizygous for *SRK01* were emasculated one
438 day before anthesis, and manually pollinated 24h later with paternal plants hemizygous for *SCR01,*
439 *SCR01*^{*mir1887}, *SCR01* Ah04mir1887 or *SCR01*^{*mir1887} Ah20mirS3. Pollinated pistils were transferred to
440 fixing solution 6h after pollination and stained with aniline blue, as described before (19). These pistils
441 were then mounted on microscope slides and imaged using a Zeiss AX10 fluorescence microscope,
442 where we counted the number of germinated pollen grains present in each pistil.

443 To evaluate the effect of RdDM mutants on the activity of *S*-locus sRNA precursors we crossed the
444 RdDM mutants *ago4 ago6*, *polIV* and *polV* with the previously described paternal plants carrying *SCR01*
445 and sRNA precursors (*SCR01, SCR01*^{*mir1887}, *SCR01* Ah04mir1887 and *SCR01*^{*mir1887} Ah20mirS3). We
446 then obtained plants hemizygous for the *SCR01* and sRNA precursor transgenes and homozygous for
447 the mutations of interest and used these as paternal plants in crosses with maternal hemizygous *SRK01*
448 plants, as described above.
449 As a control, all maternal and paternal lines used in this study were crossed to wt C24. Germination
450 and seed set for all these genotypes were comparable to that of wt x wt crosses (data not shown),
451 confirming that the transgenes and mutations had no detectable effect on plant fertility.

452 *Phenotypic determination of the S-loci dominance hierarchy*

453 The *S*-locus dominance hierarchy in **Figure 3** is based on a compilation of controlled reciprocal
454 crosses between different *A. halleri* individuals (10, 19, 35, 62). In cases where interactions between
455 alleles of two different dominance classes had not been tested phenotypically, dominance was inferred
456 based on the phylogenetic class of each allele, since interclass dominance interactions are predictable
457 (7, 16). In the case of intraclass relationships, such as for alleles Ah65, Ah60 and Ah33 (all belonging
458 to class III), phenotypic dominance has not been determined yet, and thus the ordering of these alleles
459 along the hierarchy remains arbitrary at this stage.

460 *RT-qPCR*

461 To measure the abundance of *SCR01* transcripts, we isolated immature buds of plants hemizygous
462 for *SCR01, SCR01*^{*mir1887}, *SCR01* Ah04mir1887 or *SCR01*^{*mir1887} Ah20mirS3. RNA was extracted using
463 the NucleoSpin RNA Plus kit (Macherey-Nagel) and cDNA was synthesized with the RevertAid First
464 Strand cDNA Synthesis Kit (Thermo Scientific). qPCR was performed using the iTaq Universal SYBR
465 Green Supermix (BioRad) in a Lightcycler 480 instrument (Roche), with the primers found in **table S1**.
466 *ACT8* was used as a reference gene. Transcript abundance was quantified using the Pfaffl method
467 (63).

468 *ARGONAUTE immunoprecipitation and sRNA sequencing*

469 AGO1 and AGO4 immunoprecipitation (IP) assays were performed on immature buds of *A. thaliana*
470 plants carrying homozygous Ah04mir1887 or Ah20mirS3 transgenes, using a previously published
471 protocol (64), with the following modifications: IPs were performed on 1.4 g of finely ground powder of
472 frozen immature buds. The anti-AGO1 (AS09 527, Agrisera) and anti-AGO4 (AS09 617, Agrisera)
473 antibodies were added at a 1/500 dilution for the incubation step and their immobilization was performed
474 using Dynabeads Protein G (Invitrogen). The IP products were washed six times with PBS prior to sRNA
475 extraction using the Trizol reagent (Ambion). In parallel, an aliquot of each input extract was used for
476 total sRNA isolation using the Trizol LS reagent (Invitrogen), according to the supplier instructions. For
477 each genotype three sRNA fractions were obtained: AGO1-IP, AGO4-IP and input.
478 These three sRNA fractions were subjected to an acrylamide gel-based size selection for sRNAs.
479 These sRNAs were then used for TruSeq Small RNA (Illumina) library preparation and sequenced on

480 a NextSeq 500 platform (Illumina), using 75 bp single-reads. Reads were trimmed, quality filtered, and
481 size-selected using TrimGalore (65). We followed a two-step mapping procedure with ShortStack
482 (allowing for one mismatch) (66), where we mapped sRNAs from each sample to the *A. thaliana* TAIR10
483 genome (masking the *S*-locus region), and to the sequence of the corresponding *A. halleri S*-allele
484 (Ah04, for samples carrying Ah04mir1887 and Ah20 for samples carrying Ah20mirS3). Only reads that
485 mapped exclusively to the *S*-locus were kept for further analysis. sRNA read counts were normalized
486 to rpm to allow comparison of abundance levels across samples.
487 AGO loading was inferred based on the ratio of reads found in the AGO1-IP fraction and the AGO4-
488 IP fraction: a sRNA was considered to be loaded in AGO1 or AGO4 when more than 50% of its total
489 reads were derived from either the AGO1-IP fraction or the AGO4-IP fraction, respectively. A given
490 sRNA was classified as having an unknown loading when no reads were found in both AGO-IP
491 fractions, or when the amount of reads found in the input fraction was superior to that found in any of
492 the two AGO-IP fractions.

493 *sRNA database construction and target site inference for Ah04mir1887 and Ah20mirS3*

494 To identify sRNA target sites within *SCR* genomic regions, we first compiled a comprehensive
495 database incorporating all sRNAs sequenced in the AGO-IP experiments described above, along with
496 previously sequenced sRNAs (19). This database represents the complete set of sRNAs sequenced to
497 date in our lab, and originating both from *A. thaliana* and *A. halleri* plants carrying Ah04mir1887 or
498 Ah20mirS3. In parallel, a database containing *SCR* genomic regions of different *A. halleri S*-loci was
499 compiled. This included alleles from all four dominance classes, and comprised previously published
500 sequencing data **(see *Data Availability* section for a complete list of data sources)**. In addition to
501 this, long read Nanopore sequences newly obtained from individuals carrying alleles Ah65, Ah60, Ah03,
502 Ah33 and Ah19 were also added to this database **(see section *DNA extraction, Nanopore*
503 *sequencing and assembly of S-alleles* for more details)**.
504 Using the databases of sRNA sequences and *SCR* alleles, we applied a previously published
505 homology detection algorithm (19) to find target sites. Functional sRNAs are defined as those with a
506 homology score of ≥ 18, since this score has been consistently shown to be associated with a decrease
507 in *SCR* transcript abundance of the targeted allele (10, 19). The identified sRNA - *SCR* interactions
508 were then represented in a heatmap **(Fig. 4)** using ComplexHeatmap (67), and in a circos plot **(Fig. 5)**
509 using circlize (68).

510 *DNA extraction, Nanopore sequencing and assembly of S-alleles*

511 To obtain the *S*-locus sequences of alleles Ah65, Ah60, Ah03, Ah33 and Ah19, 2 g of fresh leaves
512 were collected from five different individuals carrying these alleles and flash-frozen. High molecular
513 weight genomic DNA was extracted as described before (69). Long read sequences were obtained by
514 Oxford Nanopore Technologies (ONT) flowcells v9. To polish the contigs obtained by long read
515 sequencing Illumina data were also generated (with no step of PCR amplification to minimize
516 sequencing bias).

517 For Nanopore library preparation, the smallest genomic DNA fragments were first eliminated using
518 the Short Read Eliminator Kit (Pacific Biosciences). Libraries were then prepared according to the
519 protocol 1D Native barcoding genomic DNA (with EXP-NBD104 and SQK-LSK109) provided by Oxford
520 Nanopore Technologies. Depending on how many samples were pooled, 250 ng (pool of 9 samples) to
521 1 µg (pool of 4 samples) of genomic DNA fragments were repaired and end-prepped with the NEBNext
522 FFPE DNA Repair Mix and the NEBNext Ultra II End Repair/dA-Tailing Module (New England Biolabs).
523 Barcodes provided by ONT were then ligated using the Blunt/TA Ligase Master Mix (NEB). Barcoded
524 fragments were purified with AMPure XP beads (Beckmann Coulter), then pooled and ONT adapters
525 were added using the NEBNext Quick Ligation Module (NEB). After purification with AMPure XP beads
526 (Beckmann Coulter), each library was mixed with the sequencing buffer (ONT) and the loading beads
527 (ONT) and loaded on a PromethION R9.4.1 flow cell. In order to maintain the translocation speed, flow
528 cells were refueled with 250 µl Flush Buffer when necessary. Reads were basecalled using Guppy
529 version 3.2.10, 4.0.11, 5.0.12, 5.0.13, 5.0.16 or 5.1.12. The Nanopore long reads were not cleaned and
530 raw reads were used for genome assembly.
531 For Illumina PCR-free library preparation, 1.5 µg of genomic DNA was sonicated to a 100–1500-bp
532 size range using a Covaris E220 sonicator (Covaris). The fragments (1µg) were end-prepped, and
533 Illumina adapters (NEXTFLEX Unique Dual Index Barcodes, Perkin Elmer) were added using the Kapa
534 Hyper Prep Kit (Roche). The ligation products were purified twice with 1X AMPure XP beads (Beckman
535 Coulter). The libraries were then quantified by qPCR using the KAPA Library Quantification Kit for
536 Illumina Libraries (Roche), and their profiles were assessed on an Agilent Bioanalyzer (Agilent
537 Technologies). The libraries were sequenced on an Illumina NovaSeq 6000 instrument (Illumina) using
538 150 base-length read chemistry in a paired-end mode.
539 Nanopore sequencing data were assembled using Necat (70) with a genome size of 240 Mbp and
540 the remaining parameters left as default. Contigs produced by Necat were polished one time using
541 Racon (71) with Nanopore reads, then one time with Medaka
542 (https://github.com/nanoporetech/medaka, model r941_prom_hac_g507) and Nanopore reads, and
543 two times with Hapo-G v1.3.4 (72) and Illumina short reads. However, the cumulative sizes of our long-
544 read assemblies were larger than the estimated 240 Mb, suggesting that the assembly size was
545 currently inflated by the presence of allelic duplications. Thus, HaploMerger2 (73) was run (Batch A
546 twice to remove major misjoin and one Batch B) to generate a haploid version of each assembly.
547 To detect the *S*-locus region in the generated assemblies, blast searches were performed using the
548 genes flanking the *S*-locus (*ARK3* and *U-box* (15)) as queries. This allowed us to precisely narrow down
549 the genomic regions corresponding to the full Ah65, Ah60, Ah03, Ah33 and Ah19 *S*-alleles. We
550 annotated *SRK* using blast searches, and following Goubet et al. (15), we used Fgenesh+ (74) to predict
551 the genomic sequence of *SCR* based on a database of SCR protein sequences from already known S-
552 alleles.

553 *Determination of the* SCR01 *transcription start site (TSS)*

554 To identify the TSS of *SCR01* in *A. halleri*, total RNA was extracted from unopened buds of three
555 individuals plants from accession Zapa12 (Central Europe), Bara01 and Firi03 (Romania), genotyped

as homozygous for the Ah01 allele. A library was directly prepared using the NEBNext Ultra II Directional RNA Library Prep for Illumina Kit. Libraries were sequenced with an Illumina NovaSeq 6000 instrument (Illumina) using a paired-end 151 bp read chemistry. Short Illumina reads were bioinformatically processed to remove adapters and primer sequences, only reads ≥ 30 nucleotides were retained. These filtering steps were done using in-house-designed software based on the FastX package (75). Finally, read pairs that mapped to ribosomal sequences were filtered using SortMeRNA as previously described (76). Processed reads were aligned with STAR (77) using –alignIntronMax 3000 and –alignMatesGapMac 10000 parameters to avoid very long splicing assignment errors due to a mammalian-based design of the STAR algorithm. The vertical coverage at each base pair for the three replicates was computed using samtools depth (78) and then plotted in R after feature scaling and smoothing the curves using mean coverage values in 20 bp sliding windows.

Data availability

The AGO-IP and sRNA sequencing data is deposited in the Gene Expression Omnibus database, under the SubSeries reference GSE249507.

The Illumina and Oxford Nanopore sequencing data of the five *A. halleri* individuals carrying alleles Ah65, Ah60, Ah03, Ah33 and Ah19 are available in the European Nucleotide Archive, under the project number PRJEB70880.

The RNA-seq data used to infer the *SCR01* transcription start site are available at ENA-EBI under the following accession numbers ERR14765081, ERR14765082 and ERR14765083.

The *S*-locus sequences used in this study are a combination of previously published data (15, 19) and data generated in this study. All allele sequences can be found in GenBank, under the following references: Ah01 - this study, PP396894; Ah02 - this study, PP396895; Ah03 - this study, PP537897; Ah04 - KJ461484; Ah10 - KM592810 and KM592817; Ah12 - KJ772373 and KJ772377; Ah13 - KJ461479 and KJ461483; Ah19 - this study, PP537898; Ah20 - FO203486; Ah25 - this study, PP396896; Ah28 - KJ461478; Ah29 - KM592803; Ah33 - this study, PP537899; Ah60 - this study, PP537900; Ah65 - this study, PP537901.

Acknowledgments

This work was supported by a European Molecular Biology Organization (EMBO) Postdoctoral Fellowship attributed to RAB, by the European Research Council (NOVEL project, grant #648321) and by the French National Research Agency (TE-MoMa project, grant ANR-18-CE02-0020-01). This work was performed using the infrastructure and technical support of the Plateforme Serre, Cultures et Terrains Expérimentaux - Université de Lille for the greenhouse/field facilities. Research at the Lagrange laboratory was supported by the Centre National de la Recherche Scientifique (CNRS) and Université de Perpignan Via Domitia (UPVD). This study is set within the framework of the "Laboratoires d'Excellences (LABEX)" TULIP (ANR-10-LABX-41) and the "Ecole Universitaire de Recherche" (EUR) TULIP-GS (ANR-18-EURE-0019). Research at the Krämer laboratory was supported by the Deutsche Forschungsgemeinschaft DFG in SPP 1529 (ADAPTOMICS, Kr1967/10-1,-2), and by ERC-AdG LEAP-

EXTREME (788380). We thank Hervé Vaucheret, Vincent Colot, Claudia Köhler and Nicolas Butel for helpful discussions, and Hervé Vaucheret for sharing seeds.

References

1. J. Huang, *et al.*, Stigma receptors control intraspecies and interspecies barriers in Brassicaceae. *Nature* **614**, 303–308 (2023).

2. C. Liu, *et al.*, Pollen PCP-B peptides unlock a stigma peptide–receptor kinase gating mechanism for pollination. *Science* **372**, 171–175 (2021).

3. J. B. Nasrallah, Stop and go signals at the stigma–pollen interface of the Brassicaceae. *Plant Physiol.* kiad301 (2023). https://doi.org/10.1093/plphys/kiad301.

4. J. B. Nasrallah, "Self-incompatibility in the Brassicaceae: Regulation and mechanism of self-recognition" in *Current Topics in Developmental Biology*, (Academic Press, 2019), pp. 435–452.

5. L. Zhang, *et al.*, FERONIA receptor kinase-regulated reactive oxygen species mediate self-incompatibility in Brassica rapa. *Curr. Biol.* **31**, 3004-3016.e4 (2021).

6. V. Castric, J. Bechsgaard, M. H. Schierup, X. Vekemans, Repeated adaptive introgression at a gene under multiallelic balancing selection. *PLoS Genet.* **4** (2008).

7. M. Genete, V. Castric, X. Vekemans, Genotyping and De Novo Discovery of Allelic Variants at the Brassicaceae Self-Incompatibility Locus from Short-Read Sequencing Data. *Mol. Biol. Evol.* **37**, 1193–1201 (2020).

8. M. J. Lawrence, Population Genetics of the Homomorphic Self-incompatibility Polymorphisms in Flowering Plants. *Ann. Bot.* **85**, 221–226 (2000).

9. K. Sato, *et al.*, Coevolution of the S-Locus Genes SRK, SLG and SP11/SCR in Brassica oleracea and B. rapa. *Genetics* **162**, 931–940 (2002).

10. N. Burghgraeve, *et al.*, Base-Pairing Requirements for Small RNA-Mediated Gene Silencing of Recessive Self-Incompatibility Alleles in Arabidopsis halleri. *Genetics* **215**, genetics.303351.2020 (2020).

11. T. Kakizaki, *et al.*, Linear Dominance Relationship among Four Class-II S Haplotypes in Pollen is Determined by the Expression of SP11 in Brassica Self-Incompatibility. *Plant Cell Physiol.* **44**, 70–75 (2003).

12. H. Shiba, *et al.*, The Dominance of Alleles Controlling Self-Incompatibility in Brassica Pollen Is Regulated at the RNA Level. *Plant Cell* **14**, 491–504 (2002).

13. V. Llaurens, S. Billiard, V. Castric, X. Vekemans, Evolution of dominance in sporophytic self-incompatibility systems: I. genetic load and coevolution of levels of dominance in pollen and pistil. *Evolution* **63**, 2427–2437 (2009).

14. T. Duan, *et al.*, Dominance between self-incompatibility alleles determines the mating system of Capsella allopolyploids. [Preprint] (2023). Available at: https://www.biorxiv.org/content/10.1101/2023.04.17.537155v1 [Accessed 19 September 2023].

15. P. M. Goubet, *et al.*, Contrasted Patterns of Molecular Evolution in Dominant and Recessive Self-Incompatibility Haplotypes in Arabidopsis. *PLoS Genet.* **8**, e1002495 (2012).

16. N. L. Prigoda, A. Nassuth, B. K. Mable, Phenotypic and genotypic expression of self-incompatibility haplotypes in Arabidopsis lyrata suggests unique origin of alleles in different dominance classes. *Mol. Biol. Evol.* **22**, 1609–1620 (2005).

634 17. R. A. Fisher, The Possible Modification of the Response of the Wild Type to Recurrent Mutations.
635 *Am. Nat.* **62**, 115–126 (1928).

636 18. S. Billiard, V. Castric, Evidence for Fisher's dominance theory: How many "special cases"? *Trends*
637 *Genet.* **27**, 441–445 (2011).

638 19. E. Durand, *et al.*, Dominance hierarchy arising from the evolution of a complex small RNA
639 regulatory network. *Science* **346**, 1200–1205 (2014).

640 20. Y. Tarutani, *et al.*, Trans-acting small RNA determines dominance relationships in Brassica self-
641 incompatibility. *Nature* **466**, 983–986 (2010).

642 21. S. Yasuda, *et al.*, A complex dominance hierarchy is controlled by polymorphism of small RNAs
643 and their targets. *Nat. Plants* **3**, 1–5 (2016).

644 22. P. Chellappan, *et al.*, siRNAs from miRNA sites mediate DNA methylation of target genes. *Nucleic*
645 *Acids Res.* **38**, 6883–6894 (2010).

646 23. B. Khraiwesh, *et al.*, Transcriptional Control of Gene Expression by MicroRNAs. *Cell* **140**, 111–
647 122 (2010).

648 24. K. Panda, *et al.*, Full-length autonomous transposable elements are preferentially targeted by
649 expression-dependent forms of RNA-directed DNA methylation. *Genome Biol.* **17**, 170 (2016).

650 25. M. J. Sigman, *et al.*, An siRNA-guided ARGONAUTE protein directs RNA polymerase V to initiate
651 DNA methylation. *Nat. Plants* **7**, 1461–1474 (2021).

652 26. L. Wu, *et al.*, DNA Methylation Mediated by a MicroRNA Pathway. *Mol. Cell* **38**, 465–475 (2010).

653 27. M. E. Nasrallah, P. Liu, S. Sherman-Broyles, N. A. Boggs, J. B. Nasrallah, Natural variation in
654 expression of self-incompatibility in Arabidopsis thaliana: Implications for the evolution of selfing.
655 *Proc. Natl. Acad. Sci.* **101**, 16070–16074 (2004).

656 28. M. E. Nasrallah, P. Liu, J. B. Nasrallah, Generation of Self-Incompatible Arabidopsis thaliana by
657 Transfer of Two S Locus Genes from A. lyrata. *Science* **297**, 247–249 (2002).

658 29. N. A. Boggs, J. B. Nasrallah, M. E. Nasrallah, Independent S-Locus Mutations Caused Self-
659 Fertility in Arabidopsis thaliana. *PLoS Genet.* **5**, e1000426 (2009).

660 30. S. Fujii, *et al.*, Parallel evolution of dominant pistil-side self-incompatibility suppressors in
661 Arabidopsis. *Nat. Commun. 2020 111* **11**, 1–9 (2020).

662 31. O. Voinnet, Origin, Biogenesis, and Activity of Plant MicroRNAs. *Cell* **136**, 669–687 (2009).

663 32. X.-J. He, *et al.*, NRPD4, a protein related to the RPB4 subunit of RNA polymerase II, is a
664 component of RNA polymerases IV and V and is required for RNA-directed DNA methylation.
665 *Genes Dev.* **23**, 318–330 (2009).

666 33. S. W.-L. Chan, *et al.*, RNA Silencing Genes Control de Novo DNA Methylation. *Science* **303**,
667 1336–1336 (2004).

668 34. S. Mi, *et al.*, Sorting of Small RNAs into Arabidopsis Argonaute Complexes Is Directed by the 5′
669 Terminal Nucleotide. *Cell* **133**, 116–127 (2008).

670 35. A. Le Vève, "Balancing selection, genetic load and dominance between self-incompatibility alleles
671 in Arabidopsis : an empirical and theoretical study of this ménage à trois," Université de Lille
672 (2022-....). (2022).

673 36. H. Liu, *et al.*, Nuclear functions of mammalian MicroRNAs in gene regulation, immunity and
674 cancer. *Mol. Cancer* **17**, 64 (2018).

675 37. J. O'Brien, H. Hayder, Y. Zayed, C. Peng, Overview of MicroRNA Biogenesis, Mechanisms of
676 Actions, and Circulation. *Front. Endocrinol.* **9** (2018).

677 38. T. C. Roberts, The MicroRNA Biology of the Mammalian Nucleus. *Mol. Ther. - Nucleic Acids* **3**
678 (2014).

679 39. P. Hoffer, *et al.*, Posttranscriptional gene silencing in nuclei. *Proc. Natl. Acad. Sci.* **108**, 409–414
680 (2011).

681 40. N. G. Bologna, *et al.*, Nucleo-cytosolic Shuttling of ARGONAUTE1 Prompts a Revised Model of
682 the Plant MicroRNA Pathway. *Mol. Cell* **69**, 709-719.e5 (2018).

683 41. Y. Fang, D. L. Spector, Identification of Nuclear Dicing Bodies Containing Proteins for MicroRNA
684 Biogenesis in Living Arabidopsis Plants. *Curr. Biol.* **17**, 818–823 (2007).

685 42. W. Wang, *et al.*, An Importin β Protein Negatively Regulates MicroRNA Activity in Arabidopsis[W].
686 *Plant Cell* **23**, 3565–3576 (2011).

687 43. N. Baumberger, D. C. Baulcombe, *Arabidopsis* ARGONAUTE1 is an RNA Slicer that selectively
688 recruits microRNAs and short interfering RNAs. *Proc. Natl. Acad. Sci.* **102**, 11928–11933 (2005).

689 44. J. Dolata, *et al.*, Salt Stress Reveals a New Role for ARGONAUTE1 in miRNA Biogenesis at the
690 Transcriptional and Posttranscriptional Levels. *Plant Physiol.* **172**, 297–312 (2016).

691 45. E. J. Finnegan, D. Liang, M.-B. Wang, Self-incompatibility: Smi silences through a novel sRNA
692 pathway. *Trends Plant Sci.* **16**, 238–241 (2011).

693 46. S. Fujii, K. Kubo, S. Takayama, Non-self- and self-recognition models in plant self-incompatibility.
694 *Nat. Plants* **2**, 1–9 (2016).

695 47. H. Zhao, *et al.*, Origin, loss, and regain of self-incompatibility in angiosperms. *Plant Cell* **34**, 579–
696 596 (2022).

697 48. J. Cui, C. You, X. Chen, The evolution of microRNAs in plants. *Curr. Opin. Plant Biol.* **35**, 61–67
698 (2017).

699 49. J. T. Cuperus, N. Fahlgren, J. C. Carrington, Evolution and Functional Diversification of MIRNA
700 Genes. *Plant Cell* **23**, 431–442 (2011).

701 50. N. Fahlgren, *et al.*, Microrna gene evolution in Arabidopsis lyrata and Arabidopsis thaliana. *Plant*
702 *Cell* **22**, 1074–1089 (2010).

703 51. N. Fahlgren, *et al.*, High-throughput sequencing of Arabidopsis microRNAs: Evidence for frequent
704 birth and death of MIRNA genes. *PLoS ONE* **2**, e219 (2007).

705 52. E. Allen, *et al.*, Evolution of microRNA genes by inverted duplication of target gene sequences in
706 Arabidopsis thaliana. *Nat. Genet.* **36**, 1282–1290 (2004).

707 53. H. Bastide, S. V. Saenko, M. Chouteau, M. Joron, V. Llaurens, Dominance mechanisms in
708 supergene alleles controlling butterfly wing pattern variation: insights from gene expression in
709 Heliconius numata. *Heredity* **130**, 92–98 (2023).

710 54. M. Joron, C. D. Jiggins, A. Papanicolaou, W. O. McMillan, Heliconius wing patterns: an evo-devo
711 model for understanding phenotypic diversity. *Heredity* **97**, 157–167 (2006).

712 55. R. J. Stein, *et al.*, Relationships between soil and leaf mineral composition are element-specific,
713 environment-dependent and geographically structured in the emerging model Arabidopsis halleri.
714 *New Phytol.* **213**, 1274–1286 (2017).

715 56. S. J. Clough, A. F. Bent, Floral dip: A simplified method for Agrobacterium-mediated
716 transformation of Arabidopsis thaliana. *Plant J.* **16**, 735–743 (1998).

717 57. H.-L. Xing, *et al.*, A CRISPR/Cas9 toolkit for multiplex genome editing in plants. *BMC Plant Biol.*
718 **14**, 327 (2014).

719 58. Z.-P. Wang, *et al.*, Egg cell-specific promoter-controlled CRISPR/Cas9 efficiently generates
720 homozygous mutants for multiple target genes in Arabidopsis in a single generation. *Genome*
721 *Biol.* **16**, 144 (2015).

722 59. S. Lahmy, *et al.*, Evidence for ARGONAUTE4–DNA interactions in RNA-directed DNA
723 methylation in plants. *Genes Dev.* **30**, 2565–2570 (2016).

724 60. C.-G. Duan, *et al.*, Specific but interdependent functions for Arabidopsis AGO4 and AGO6 in RNA-
725 directed DNA methylation. *EMBO J.* **34**, 581–592 (2015).

726 61. S. M. Smith, P. J. Maughan, SNP genotyping using KASPar assays. *Methods Mol. Biol. Clifton*
727 *NJ* **1245**, 243–256 (2015).

728 62. V. Llaurens, *et al.*, Does frequency-dependent selection with complex dominance interactions
729 accurately predict allelic frequencies at the self-incompatibility locus in Arabidopsis halleri?
730 *Evolution* **62**, 2545–2557 (2008).

731 63. M. W. Pfaffl, A new mathematical model for relative quantification in real-time RT-PCR. *Nucleic*
732 *Acids Res.* **29**, 45e–445 (2001).

733 64. C. Barre-Villeneuve, *et al.*, The unique dual targeting of AGO1 by two types of PRMT enzymes
734 promotes phasiRNA loading in Arabidopsis thaliana. *Nucleic Acids Res.* gkae045 (2024).
735 https://doi.org/10.1093/nar/gkae045.

736 65. F. Krueger, TrimGalore. (2016). Deposited 2016.

737 66. M. J. Axtell, ShortStack: Comprehensive annotation and quantification of small RNA genes. *RNA*
738 **19**, 740 (2013).

739 67. Z. Gu, Complex heatmap visualization. *iMeta* **1**, e43 (2022).

740 68. Z. Gu, L. Gu, R. Eils, M. Schlesner, B. Brors, circlize implements and enhances circular
741 visualization in R. *Bioinformatics* **30**, 2811–2812 (2014).

742 69. C. Belser, *et al.*, Chromosome-scale assemblies of plant genomes using nanopore long reads
743 and optical maps. *Nat. Plants* **4**, 879–887 (2018).

744 70. Y. Chen, *et al.*, Efficient assembly of nanopore reads via highly accurate and intact error
745 correction. *Nat. Commun.* **12**, 60 (2021).

746 71. R. Vaser, I. Sović, N. Nagarajan, M. Šikić, Fast and accurate de novo genome assembly from
747 long uncorrected reads. *Genome Res.* **27**, 737–746 (2017).

748 72. J.-M. Aury, B. Istace, Hapo-G, haplotype-aware polishing of genome assemblies with accurate
749 reads. *NAR Genomics Bioinforma.* **3**, lqab034 (2021).

750 73. S. Huang, M. Kang, A. Xu, HaploMerger2: rebuilding both haploid sub-assemblies from high-
751 heterozygosity diploid genome assembly. *Bioinformatics* **33**, 2577–2579 (2017).

752 74. V. Solovyev, P. Kosarev, I. Seledsov, D. Vorobyev, Automatic annotation of eukaryotic genes,
753 pseudogenes and promoters. *Genome Biol.* **7**, S10 (2006).

754 75. C. Belser, *et al.*, Integrative omics framework for characterization of coral reef ecosystems from
755 the Tara Pacific expedition. *Sci. Data* **10**, 326 (2023).

756 76. R. Li, Y. Li, K. Kristiansen, J. Wang, SOAP: short oligonucleotide alignment program.
757 *Bioinformatics* **24**, 713–714 (2008).

758 77. A. Dobin, *et al.*, STAR: ultrafast universal RNA-seq aligner. *Bioinforma. Oxf. Engl.* **29**, 15–21
759 (2013).

760 78. P. Danecek, *et al.*, Twelve years of SAMtools and BCFtools. *GigaScience* **10**, giab008 (2021).

761

762

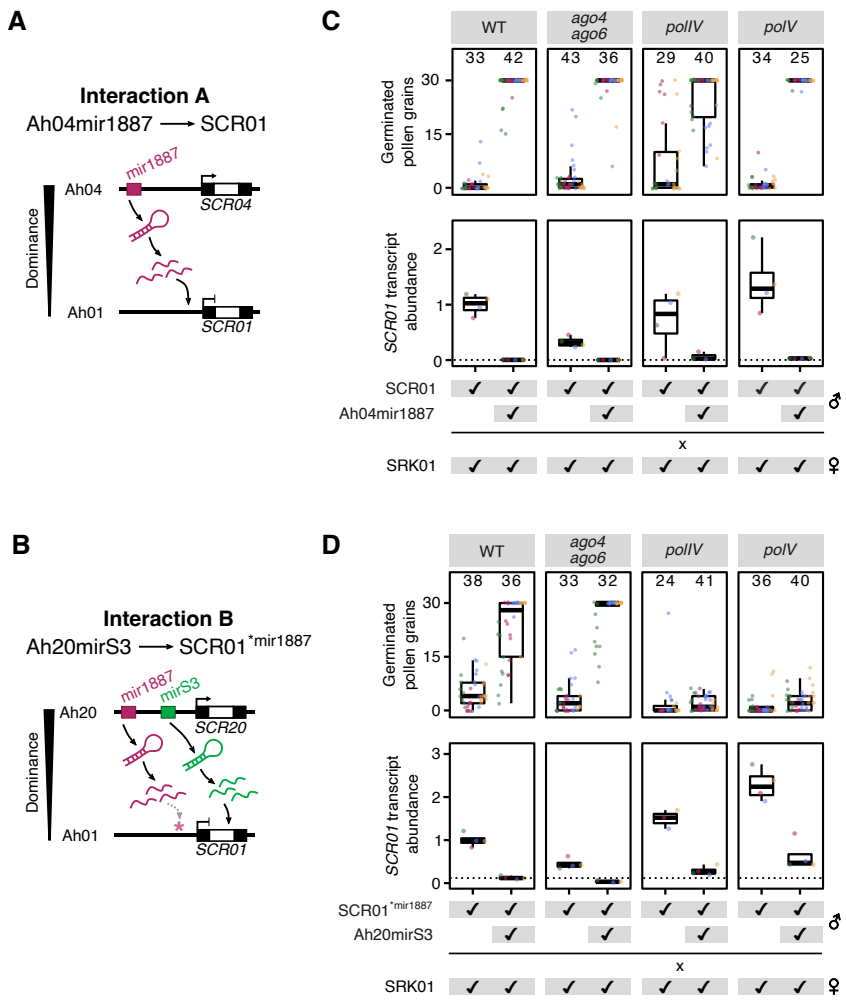

Figure 1. The RdDM pathway is not required for the activity of Ah04mir1887 and Ah20mirS3.

(A,B) Dominance interactions studied in this paper. The black and white regions within *SCR* genes correspond to exons and introns, respectively. **(A)** Interaction A focuses on the role of the sRNA precursor Ah04mir1887 in mediating the dominance of Ah04 over Ah01. **(B)** Interaction B focuses on the role of Ah20mirS3 in mediating the dominance of Ah20 over Ah01. *S*-locus sRNA precursors consist of inverted repeats that form hairpins which are processed into multiple sRNAs showing sequence homology to specific *SCR* regions: Ah04mir1887 sRNAs show homology to the 5' region region of *SCR01*, while Ah20mirS3 sRNAs show homology to the intronic region (white) of *SCR01*. Because sRNAs produced from the Ah20mir1887 precursor show homology to the wt *SCR01* 5' region region, and to study the specific effect of Ah20mirS3 in Interaction B, the *SCR01*^{*mir1887} line containing five point mutations in the *SCR01* 5' region was created, which disrupts the homology with Ah20mir1887 sRNAs. **(C,D)** Phenotypic and expression assay evaluating the role of key RdDM components on the action of Ah04mir1887 **(C)**, and Ah20mirS3 **(D)**. Crosses between *SRK01*-expressing mothers and *SCR01*-expressing fathers were performed in wt and RdDM mutant backgrounds in the absence or presence of the respective sRNA precursor. The number of germinated pollen grains of the indicated genotype was counted on pistils of SRK01 mothers. *SCR01* expression in immature buds of the indicated genotype was measured by RT-qPCR and normalized to the wt level. Five biological replicates

780 (represented by the differently colored dots) were analyzed for pollen germination and *SCR01*
781 expression. Numbers on top of columns indicate the total number of siliques sampled for pollen
782 germination assays.

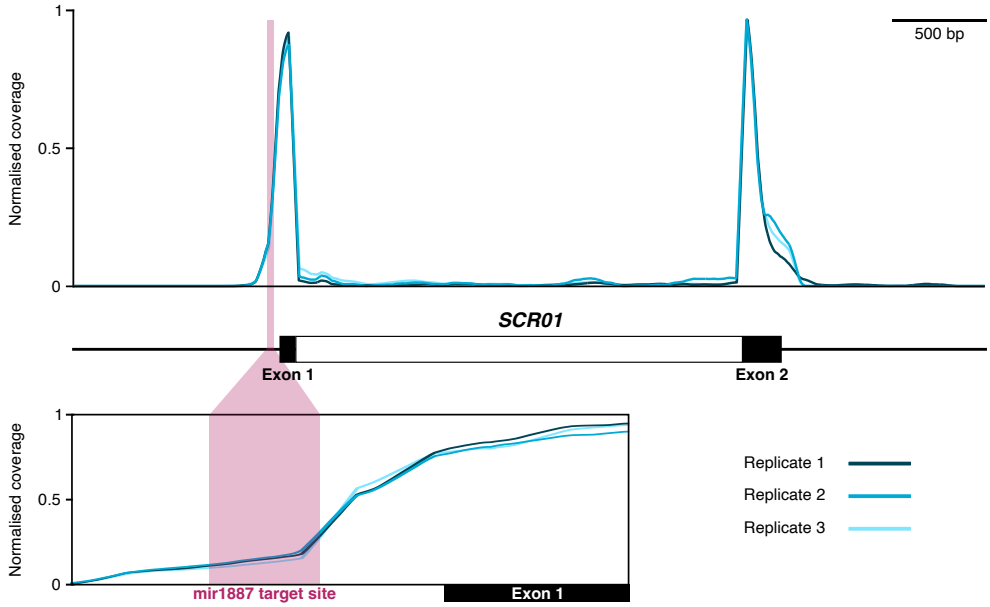

783 **Figure 1 S1. SCR TSS in relation to Ah04mir1887 target site.**

784 Normalised RNA-seq coverage along the *SCR01* sequence from three biological replicates of
785 homozygous *Ah01* allele plants. Exons and introns within *SCR01* gene are represented by black and
786 white regions, respectively. The *mir1887* target site is highlighted in light red and the bottom panel
787 provides a magnified view of this site, including the flanking exon 1. The three replicates are depicted
788 as curves in different shades of blue. Raw vertical coverage distributions (number of aligned reads at
789 each position) are normalized to the maximum value for each replicate. The curves are smoothed using
790 a 20 bp sliding window, advancing by 1 bp per step.

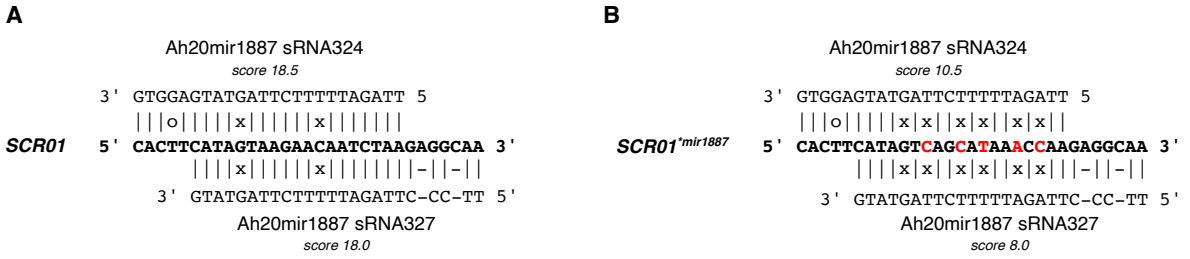

Figure 1 S2. *SCR01*mir1887* transgenic line. (A) Alignment between the native mir1887 target site on SCR01 and Ah20mir1887 sRNAs with a targeting score ≥ 18. **(B)** Alignment between the same sRNAs and the mutated mir1887 target site of the transgenic line SCR01*mir1887. Note that the mutations decrease the homology score below 18, suggesting that these sRNAs are not able to target the mutated site. Mutated sites are in red.

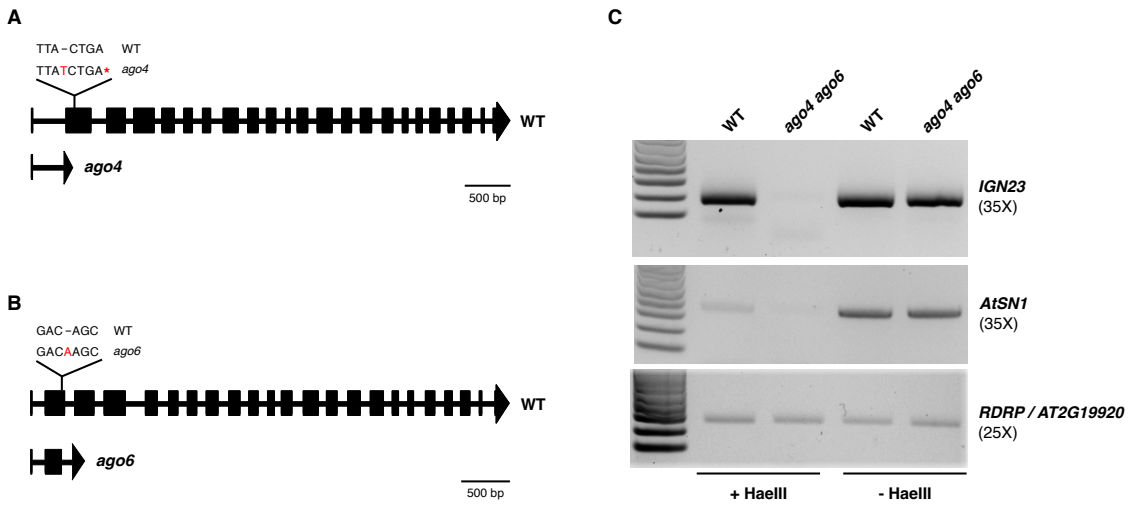

Figure 1 S3. Validation of the RdDM CRISPR/Cas9 mutants generated in this study.

(A-B) Schematic representation of CRISPR/Cas9 induced mutations in the *AGO4* and *AGO6* genes. Sequence changes are shown in red, premature stop codons are represented by the asterisk. **(C)** Chop-PCR assay on wt C24 plants and *ago4 ago6* double mutant plants. *IGN23* and *AtSN1* correspond to RdDM-dependent methylated regions, while *RDRP* corresponds to a non-methylated region.

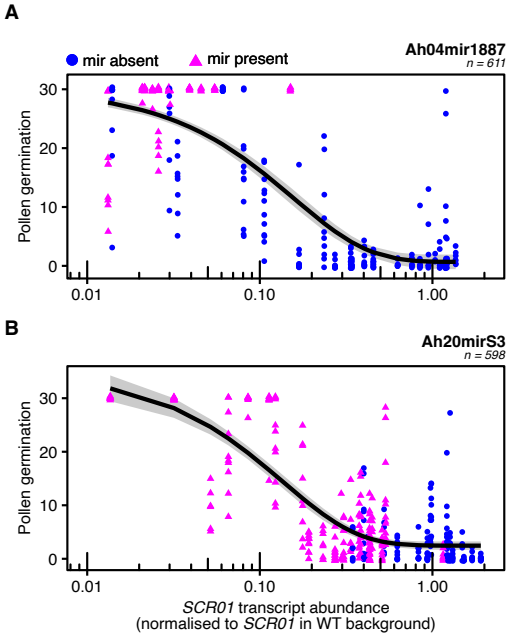

Figure 1 S4. A compatible pollen germination phenotype requires a low *SCR01* transcript abundance.

Non-linear regression analysis modeling the relationship between *SCR01* transcript abundance levels and pollen germination. For both Ah04mir1887 **(A)** and Ah20mirS3 **(B)** sRNA precursors a compatible pollen germination phenotype (~20-30 pollen grains) requires a 10-fold decrease in *SCR01* transcript abundance (compared to the level observed in the wt). Analysis was performed using the phenotypic and expression data presented in **Fig. 1 C-D**. The black line represents the predicted model and the gray area corresponds to the 95% confidence interval.

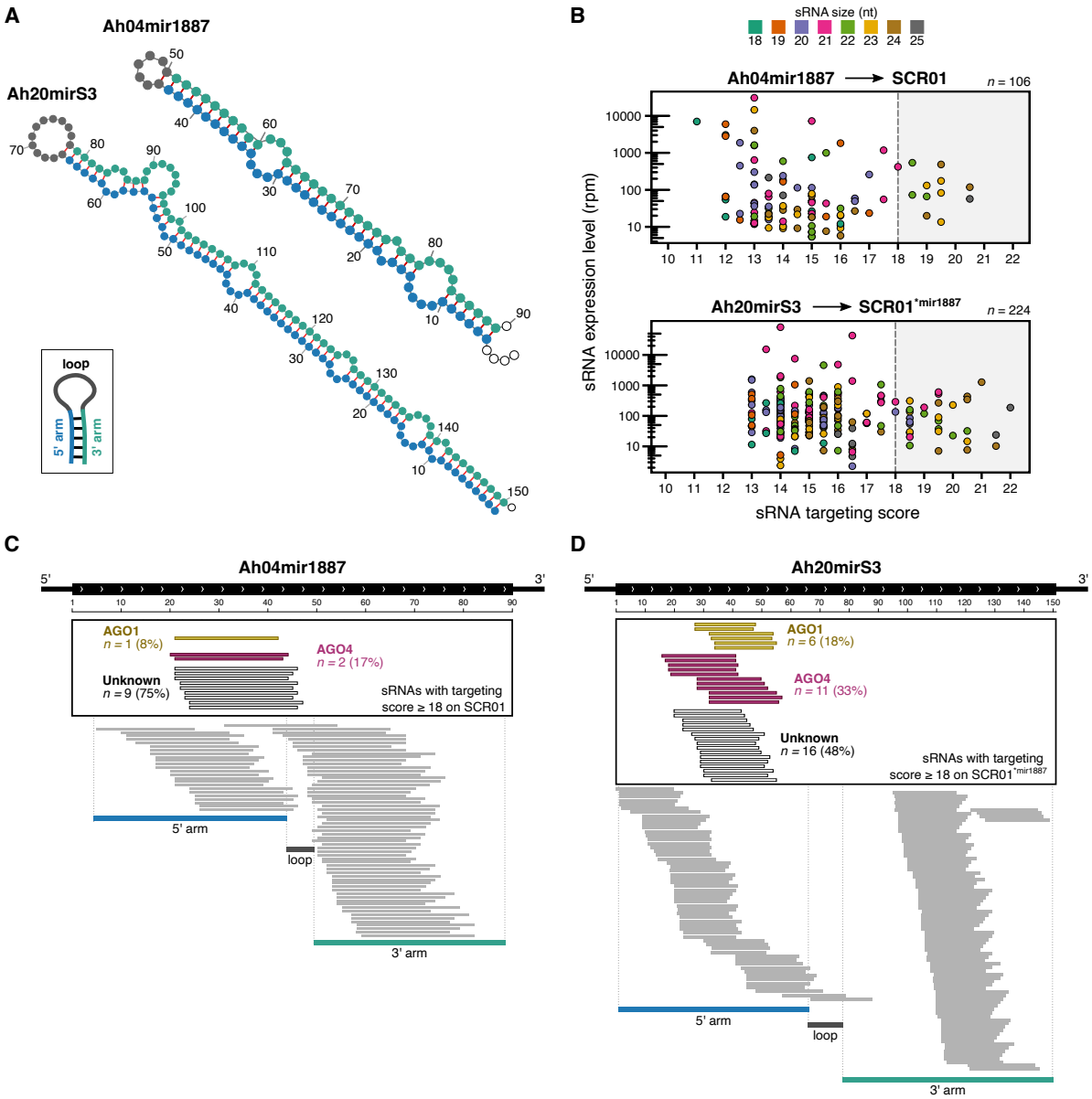

Figure 2. Ah04mir1887 and Ah20mirS3 hairpins are processed into numerous sRNAs.

(A) Predicted RNA hairpin structures of the *S*-locus sRNA precursors Ah04mir1887 and Ah20mirS3. **(B)** Expression of Ah04mir1887 and Ah20mirS3 sRNAs as a function of their targeting score against *SCR01*. The dot color corresponds to the size of the sRNA. The grey box highlights sRNAs predicted to induce a reduction in *SCR01* transcript abundance (score ≥ 18). *n* corresponds to the total number of unique sRNAs identified for each sRNA precursor. **(C-D)** Genomic representation of the Ah04mir1887 and Ah20mirS3 loci, and their respective sRNAs. The black rectangle highlights sRNAs predicted to induce a reduction in *SCR01* transcript abundance (score ≥ 18). AGO loading information for each functional sRNA is indicated by the sRNA color (yellow – sRNA loaded predominantly in AGO1; magenta – sRNA loaded predominantly in AGO4; white – sRNAs with unknown loading profile), **see Methods section *ARGONAUTE immunoprecipitation and sRNA sequencing*** for more details.

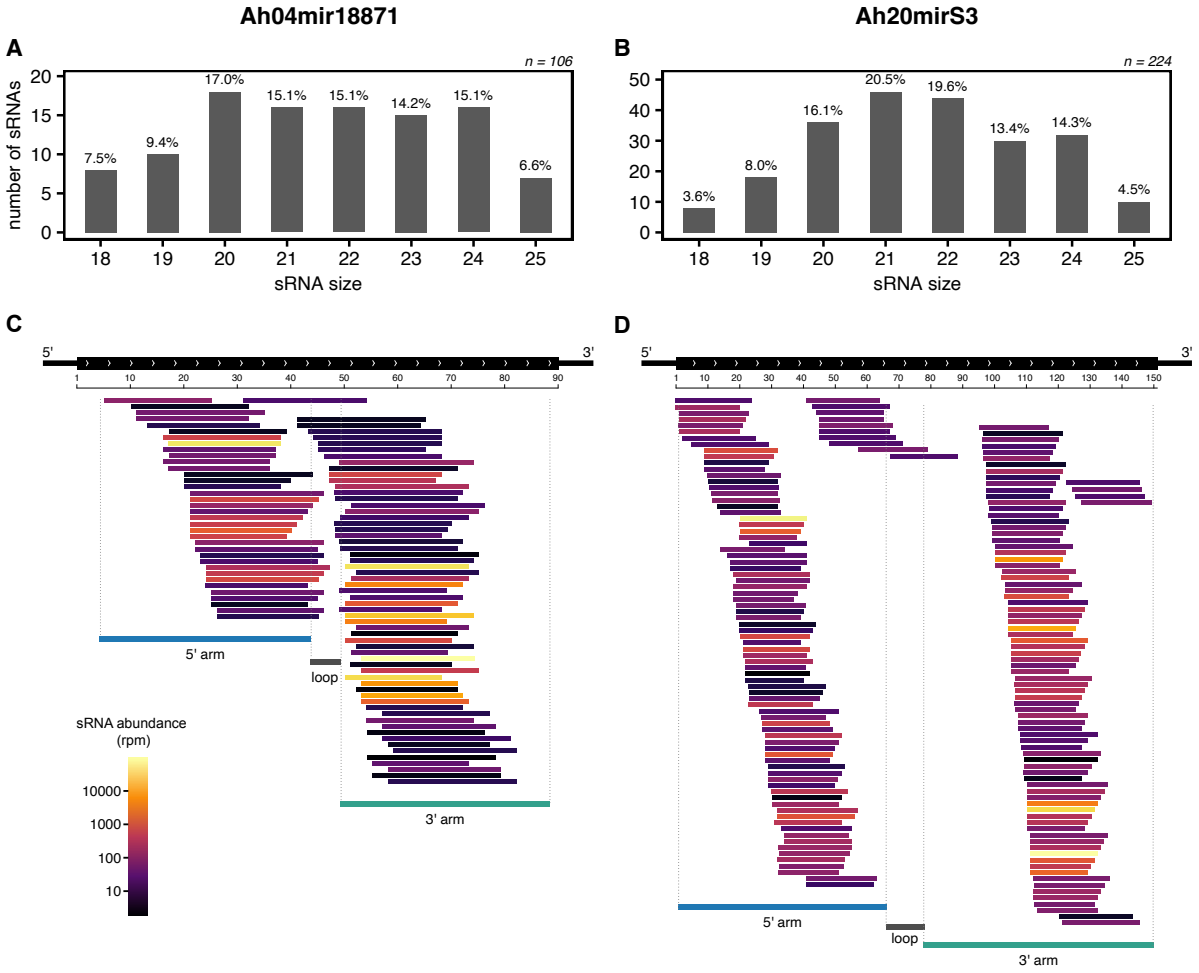

820 **Figure 2 S1. sRNAs produced from Ah04mir1887 and Ah20mirS3 do not show a specific size**
821 **bias but vary in their abundance levels.**

822 Size distribution of sRNAs derived from Ah04mir1887 **(A)** and Ah20mirS3 **(B)**. **(C-D)** Genomic
823 representation of the Ah04mir1887 and Ah20mirS3 loci, and their respective sRNAs. sRNAs are colored
824 according to their abundance level.

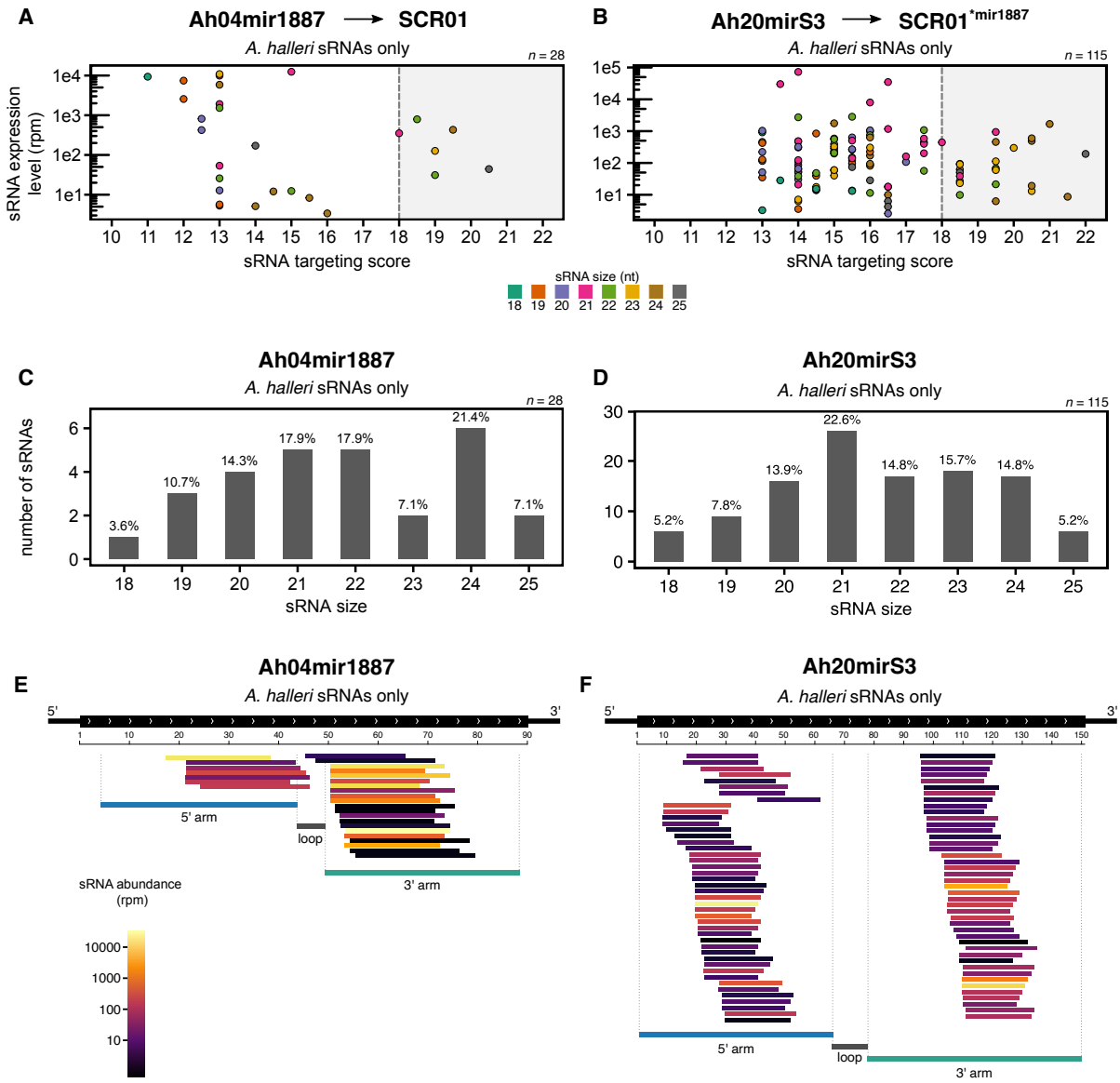

G

		A. thaliana	*A. halleri*
Nr. of sequenced samples carrying sRNA precursor of interest	Ah04mir1887	5	8
	Ah20mirS3	4	8
Total sequencing depth in sRNA precursor of interest (rpm)	Ah04mir1887	6,77E+05	1,99E+04
	Ah20mirS3	1,02E+06	6,22E+05

Figure 2 S2. Molecular features of *A. halleri*-specific sRNAs produced by Ah04mir1887 and Ah20mirS3.

(A-B) Expression of Ah04mir1887 **(A)** and Ah20mirS3 **(B)** *A. halleri* sRNAs as a function of their targeting score against *SCR01*. The dot color corresponds to the size of the sRNA. The grey box highlights sRNAs predicted to induce a reduction in *SCR01* transcript abundance (score ≥ 18). *n* corresponds to the total number of unique sRNAs identified in *A. halleri*. **(C-D)** Size distribution of *A. halleri* sRNAs derived from Ah04mir1887 **(C)** and Ah20mirS3 **(D)**. **(E-F)** Genomic representation of the

832 Ah04mir1887 **(E)** and Ah20mirS3 **(F)** loci, and the respective *A. halleri* sRNAs. sRNAs are colored
833 according to their abundance level. **(G)** Summary of sRNA sequencing efforts in *A. thaliana* transgenic
834 lines and *A. halleri* lines carrying Ah04mir1887 and Ah20mirS3.

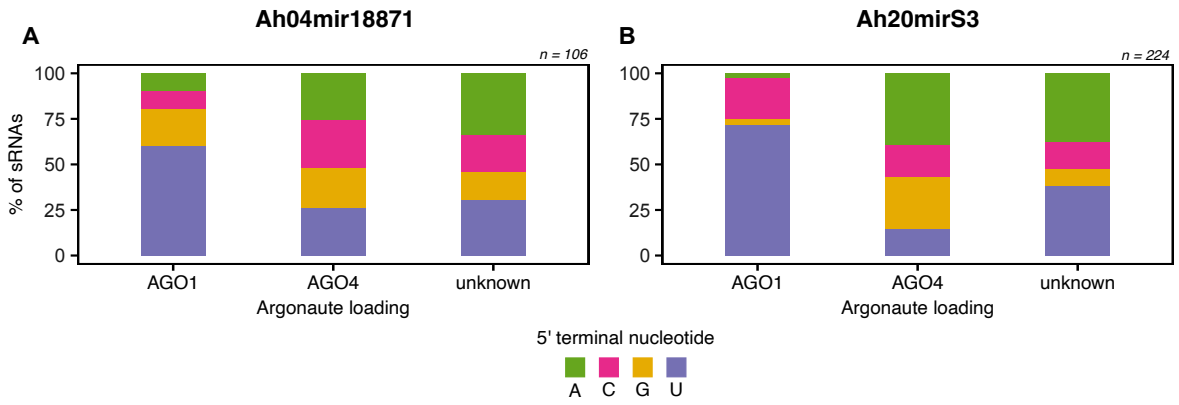

835 **Figure 2 S3. 5' terminal nucleotide frequencies in Ah04mir1887 (A) and Ah20mirS3 (B) sRNAs,**
836 **related to their inferred AGO loading pattern.**

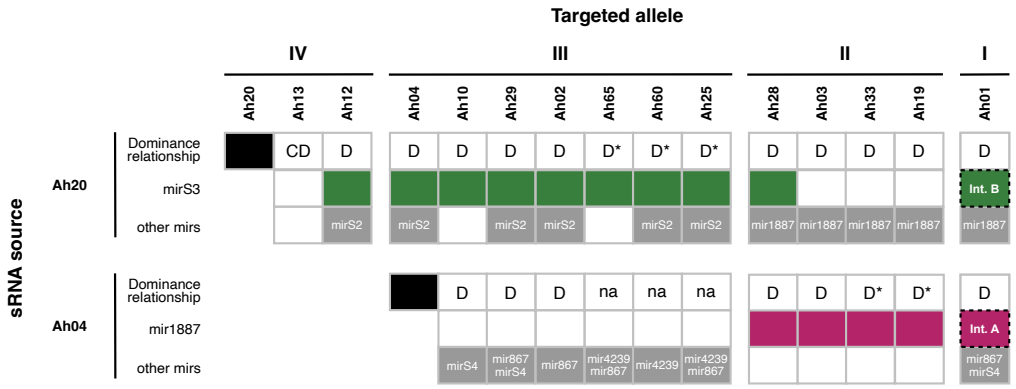

Figure 3. Ah04mir1887 and Ah20mirS3 underlie numerous *S*-allele dominance interactions.

Schematic representation of the dominance relationship between alleles Ah20, Ah04 and other *S*-alleles in the current *A. halleri* dominance network. The dominance phenotypes observed are represented by D (dominant, as determined by phenotypic assays), CD (codominant, as determined by phenotypic assays), and na (no phenotypic data available). D* refers to a predicted dominance relationship, based on the difference between the dominance class of the sRNA source and the targeted allele (7, 16). The sRNA precursors underlying each dominance relationship are highlighted in green (mirS3), magenta (mir1887), or grey (other mirs). The specific interactions studied earlier in this manuscript – Interaction A and Interaction B - are highlighted by a dashed box.

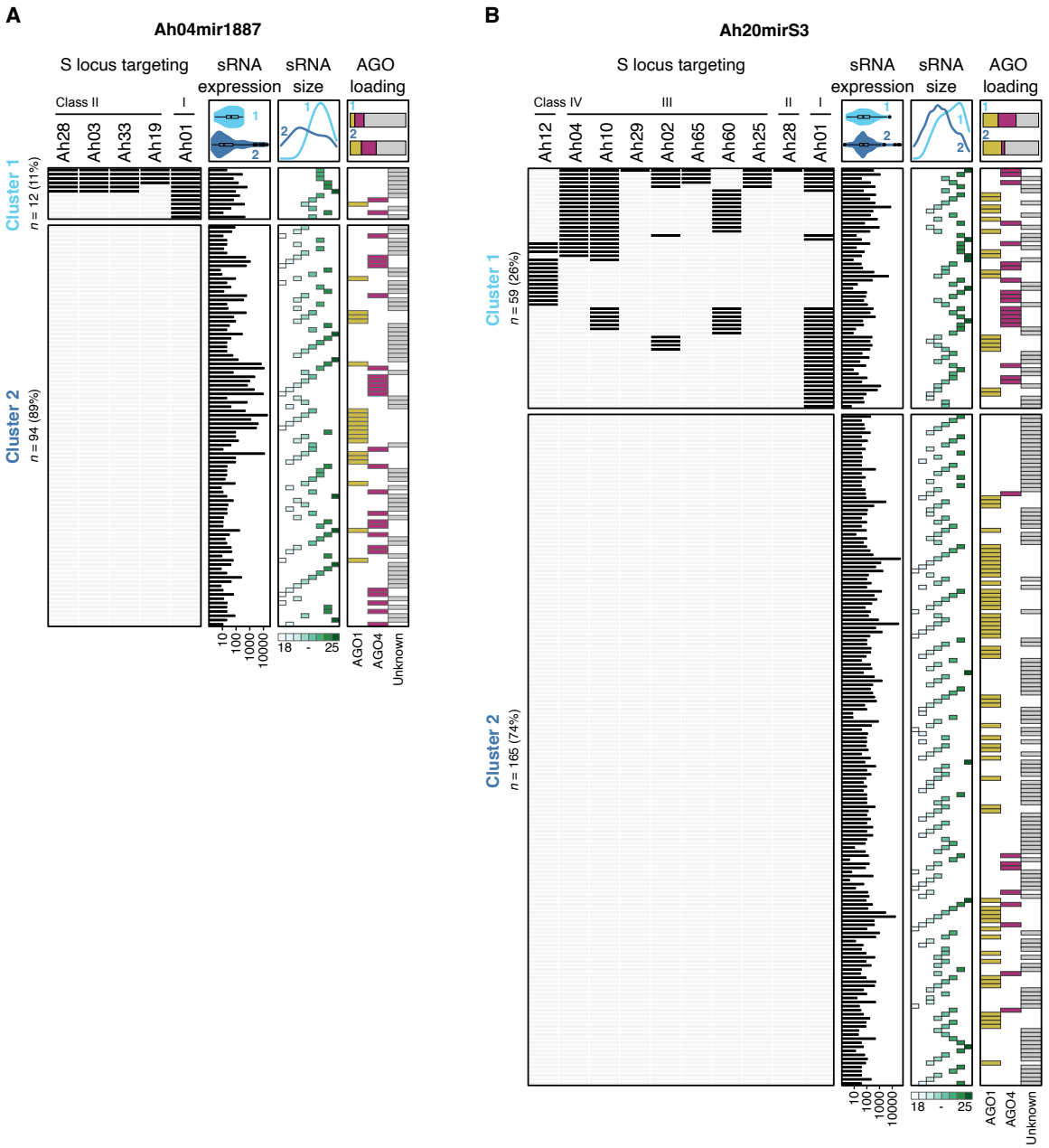

Figure 4. Ah04mir1887 and Ah20mirS3 produce multiple sRNAs predicted to target one or more *S*-alleles.

Heatmap representing the *S*-loci targeted by Ah04mir1887-derived sRNAs **(A)** and Ah20mirS3-derived sRNAs **(B)**. A black rectangle indicates that a specific sRNA has a targeting score of ≥ 18 against the corresponding *S*-allele. Cluster 1 groups sRNAs that target at least one *S*-allele, while Cluster 2 groups sRNAs that have no targets in the represented *S*-alleles. sRNA expression levels, sRNA size and AGO loading patterns are indicated for each sRNA. Summary plots comparing these features in Cluster 1 and Cluster 2 are shown in the top panel. *n* corresponds to the number of sRNAs produced by each sRNA precursor.

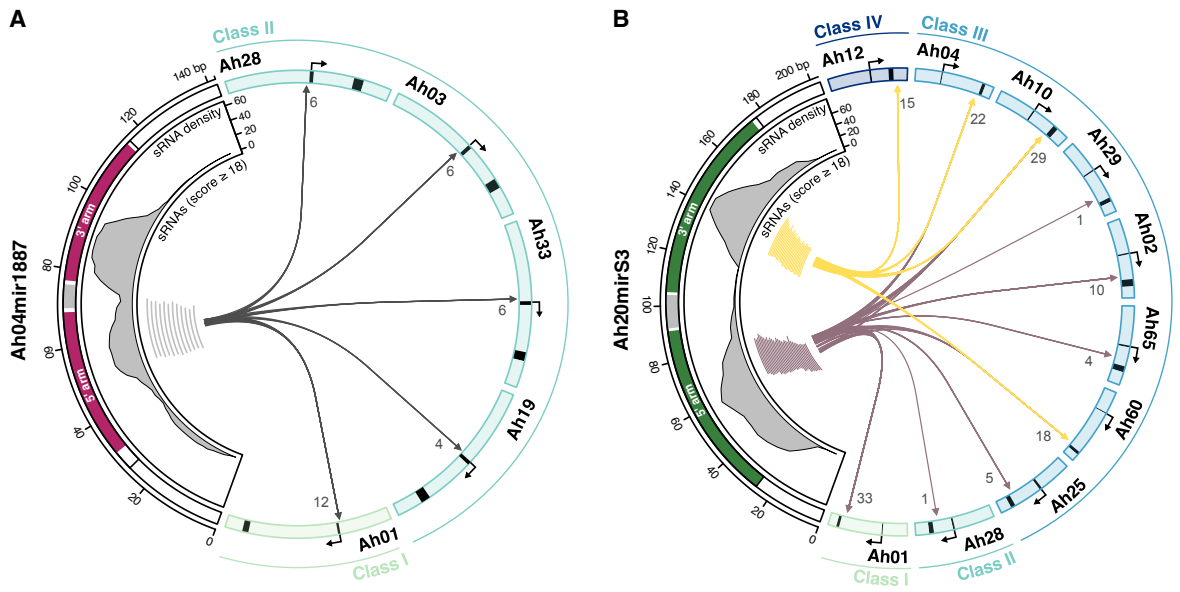

855 **Figure 5. The targeting repertoire of *S*-locus sRNA precursors is enhanced by their**
856 **heterogeneous processing pattern.**

857 Circos plot representing the positional relationship between sRNAs produced by Ah04mir1887 **(A)**,
858 Ah20mirS3 **(B)** and the corresponding targeted *S*-alleles. The genomic regions harboring Ah04mir1887
859 and Ah20mirS3 are represented on the left side of the plots. The predicted 5' and 3' hairpin arms are
860 represented in magenta (Ah04mir1887) and green (Ah20mirS3), and the sRNA density (number of
861 sRNAs) is plotted along the sRNA precursor region. Individual sRNAs with a score of ≥ 18 are
862 represented by the grey, yellow or dark purple segments. Arrowed segments represent the sRNA
863 source - target relationship. The numbers at the end of these arrowed segments indicate the total
864 number of sRNAs targeting that respective allele. The *SCR* genomic region of targeted *S*-alleles is
865 represented on the right side and includes 1500 bp upstream of the TSS and 500 bp downstream of
866 the TES. *SCR* exons 1 and 2 are colored in black.